LUND UNIVERSITY

Extending relativistic linear response theory to address solvent effects

Creutzberg, Joel

2022

Link to publication

Citation for published version (APA):
Creutzberg, J. (2022). *Extending relativistic linear response theory to address solvent effects*. Lunds Universitet/Lunds Tekniska Högskola.

Total number of authors:
1

General rights
Unless other specific re-use rights are stated the following general rights apply:
Copyright and moral rights for the publications made accessible in the public portal are retained by the authors and/or other copyright owners and it is a condition of accessing publications that users recognise and abide by the legal requirements associated with these rights.

- Users may download and print one copy of any publication from the public portal for the purpose of private study or research.
- You may not further distribute the material or use it for any profit-making activity or commercial gain
- You may freely distribute the URL identifying the publication in the public portal

Read more about Creative commons licenses: https://creativecommons.org/licenses/

Take down policy
If you believe that this document breaches copyright please contact us providing details, and we will remove access to the work immediately and investigate your claim.

LUND UNIVERSITY

PO Box 117
221 00 Lund
+46 46-222 00 00

Extending relativistic linear response theory to address solvent effects

JOEL CREUTZBERG | DIVISION OF THEORETICAL CHEMISTRY | LUND UNIVERSITY

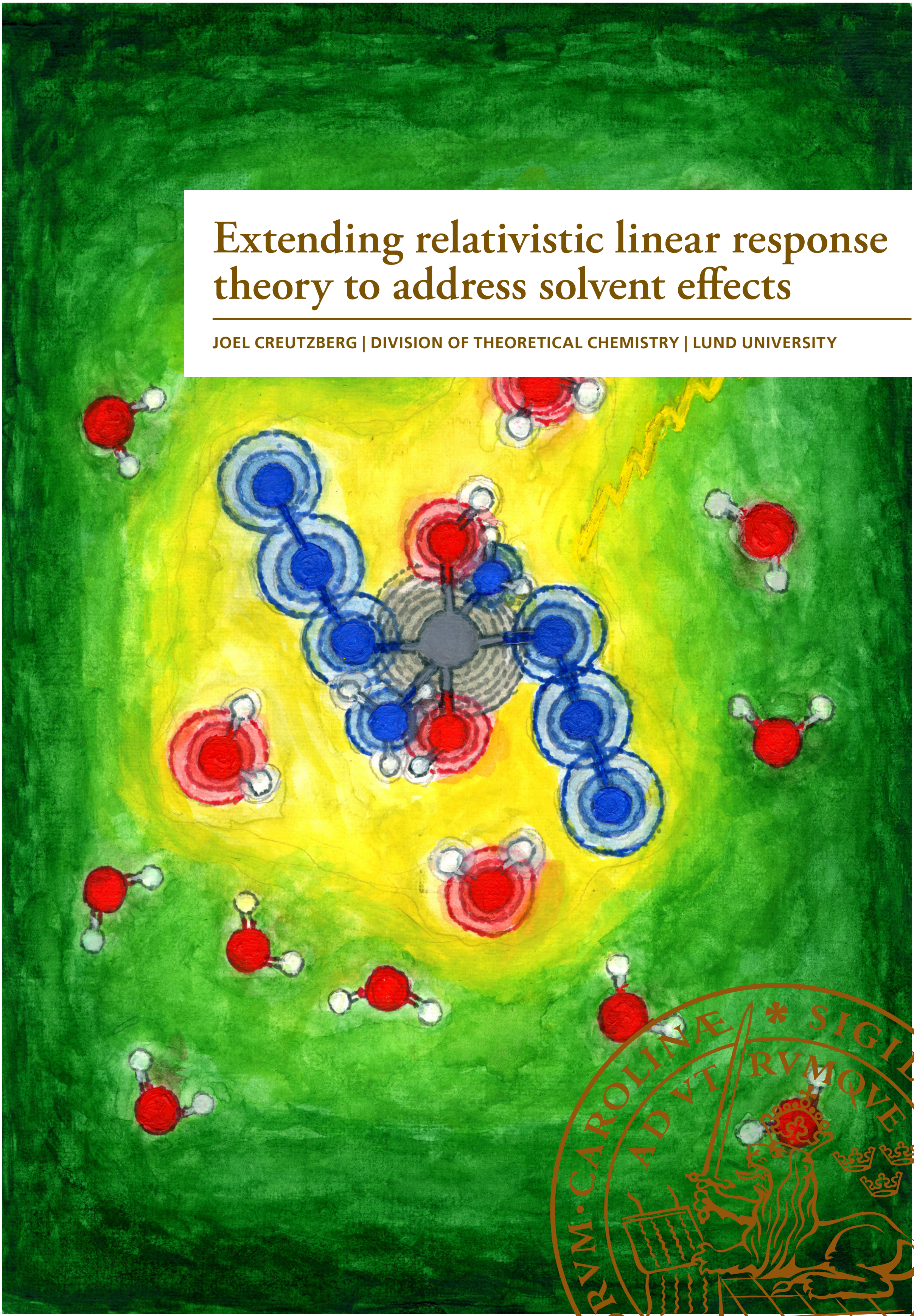

Printed by Media-Tryck, Lund 2021 NORDIC SWAN ECOLABEL 3041 0903

LUND
UNIVERSITY

ISBN: 978-91-7422-922-6

Theoretical Chemistry
Department of Chemistry
Faculty of Science
Lund University

9 789174 229226

Extending relativistic linear response theory to address solvent effects

Extending relativistic linear response theory to address solvent effects

by Joel Creutzberg

LUND
UNIVERSITY

Thesis for the degree of Doctor
Thesis advisors: Associate Professor Erik D. Hedegård, Professor Ulf Ryde
Faculty opponent: Professor Ove Christiansen

To be presented, with the permission of the Faculty of Theoretical Chemistry of Lund University, for public criticism in lecture hall A, Center for Chemistry and Chemical Engineering, Naturvetarvägen 14, Lund, on Thursday, the 15th of December 2022 at 13:00.

Organization
LUND UNIVERSITY
Department of Chemistry
Box 124
SE–221 00 LUND
Sweden

Document name
DOCTORAL DISSERTATION

Date of disputation
2022-12-15

Sponsoring organization

Author(s)
Joel Creutzberg

Title and subtitle
Extending relativistic linear response theory to address solvent effects

Abstract

The central aim of this thesis is to derive, implement and test new methods to calculate various types of spectroscopies of compounds containing heavy elements in an aqueous environment. Methods that can target such systems have to consider the following:
(i) It is crucial to take relativistic effects into account.
(ii) Modeling of larger systems is expensive in quantum chemistry. Thus, cheaper options need to be considered for the water solvent.
(iii) Methods to calculate electronic spectra have to be able to model electronic excitations properly.
(i) The relativistic effects can be obtained by solving the Dirac equation. This yields a four-component wave function, but methods based on only two-components have been developed in this thesis. (ii) Larger systems can be tackled by dividing them into a region that is treated by methods from electronic structure theory, and a larger environment that is treated classically as a collection of localized static multipole moments (charges, dipole moments, etc.). In most such hybrid schemes (called QM/MM) we only take into account how the static multipole moments in the environment influence the wave function in the QM region. In this thesis, however, we allow mutual polarization of the regions through the polarizable embedding (PE) model. (iii) We calculate excited state properties through linear response theory. This has been developed to work with a variety of approximate state wave functions and has been extended to a relativistic framework. Moreover, it has been combined with PE. Yet, regular linear response theory suffers from problems in non-resonant regions of spectra. For this, we consider a variant of linear response theory, called the complex polarization propagator. Here, the life-times of the excited states are included in the response equations. This allows the calculation of spectra in regions that are problematic in regular response theory.
In this thesis, we have devised a method that combines relativistic CPP within a polarizable embedding framework. We employ the method on light-activated platinum complexes with application in chemotheraphy. Here, both relativistic and solvent effects are crucial to model the excitation processes. Moreover, we also consider the calculation of electronic circular dichroism for chiral organic molecules that contain heavy elements like iodine.

DOKUMENTDATABLAD enl SIS 61 41 21

Key words
Response theory, Polarizable embedding, Complex polarization propagator, relativistic effects

Classification system and/or index terms (if any)

Supplementary bibliographical information

Language
English

ISSN and key title

ISBN
978-91-7422-922-6 (print)
978-91-7422-923-3 (pdf)

Recipient's notes

Number of pages
189

Price

Security classification

I, the undersigned, being the copyright owner of the abstract of the above-mentioned dissertation, hereby grant to all reference sources the permission to publish and disseminate the abstract of the above-mentioned dissertation.

Signature ______________________ Date 2022-11-04

Extending relativistic linear response theory to address solvent effects

by Joel Creutzberg

LUND
UNIVERSITY

A doctoral thesis at a university in Sweden takes either the form of a single, cohesive research study (monograph) or a summary of research papers (compilation thesis), which the PhD student has written alone or together with one or several other author(s).

In the latter case the thesis consists of two parts. An introductory text puts the research work into context and summarizes the main points of the papers. Then, the research publications themselves are reproduced, together with a description of the individual contributions of the authors. The research papers may either have been already published or are manuscripts at various stages (in press, submitted, or in draft).

Cover illustration front: Light-activation of a platinum complex with surrounding water molecules by Joel Creutzberg

Parts of this thesis have been published before in: Creutzberg, Joel, *Response theory in a relativistic polarizable embedding framework* 2021

© Joel Creutzberg 2022

Faculty of Theoretical Chemistry, Department of Chemistry

isbn: 978-91-7422-922-6 (print)
isbn: 978-91-7422-923-3 (pdf)

Printed in Sweden by Media-Tryck, Lund University, Lund 2022

Media-Tryck is a Nordic Swan Ecolabel certified provider of printed material. Read more about our environmental work at www.mediatryck.lu.se

Printed matter
3041 0903

MADE IN SWEDEN

Contents

List of publications iii
Publications not included in this thesis iv
Acknowledgements v
Populärvetenskaplig sammanfattning på svenska vi

Extending relativistic linear response theory to address solvent effects 1

1 Light-activated anti-cancer platinum complexes 3

2 Electronic structure theory 7
- 2.1 Second quantization 7
- 2.2 The molecular Schrödinger equation 8
- 2.3 The Dirac equation 9
- 2.4 Hartree-Fock theory 11
  - 2.4.1 Slater determinants 11
  - 2.4.2 Hartree-Fock equations 11
- 2.5 Kohn-Sham density functional theory 13
  - 2.5.1 KS-DFT in second quantization 14
  - 2.5.2 Exchange-correlation functionals 14

3 Polarizable embedding 17
- 3.1 QM/MM with electrostatic and polarizable embedding 17
  - 3.1.1 Electrostatic interactions with multipole expansions 18
  - 3.1.2 Induced dipole polarization 20
- 3.2 The LoProp method 22

4 Linear response theory 25
- 4.1 The quasi energy 25
- 4.2 Linear response for approximate wavefunctions 27
- 4.3 Damped linear response theory 29
- 4.4 Linear response properties 30
  - 4.4.1 UV-Vis absorption 30
  - 4.4.2 Electronic circular dichroism 31

5 Research and Outlook 33

5.1 Summaries of papers 33
5.2 Outlook 45

References 47

Scientific publications 51

Author contributions 51

Paper i: Investigating the influence of relativistic effects on absorption spectra for platinum complexes with light-activated activity against cancer cells 51

Paper ii: Polarizable embedding complex polarization propagator in a four- and two-component frameworks 51

Paper iii: New relativistic quantum chemical methods for understanding light-induced therapeutics 51

Paper iv: A method to capture the large relativistic and solvent effects on UV-vis spectra of photo-activated metal complexes . . . 51

Paper v: Electronic Circular Dichroism at the level of four-component Kohn–Sham density functional theory 52

Paper vi: A method to explore the combined impact of relativistic and solvent effects on electronic circular dichroism spectra . 52

Paper i: Investigating the influence of relativistic effects on absorption spectra for platinum complexes with light-activated activity against cancer cells 53

Paper ii: Polarizable embedding complex polarization propagator in a four- and two-component frameworks 67

Paper iii: New relativistic quantum chemical methods for understanding light-induced therapeutics 85

Paper iv: A method to capture the large relativistic and solvent effects on UV-vis spectra of photo-activated metal complexes 97

Paper v: Electronic Circular Dichroism at the level of four-component Kohn–Sham density functional theory 127

Paper vi: A method to explore the combined impact of relativistic and solvent effects on electronic circular dichroism spectra 151

List of publications

This thesis is based on the following publications, referred to by their Roman numerals:

i **Investigating the influence of relativistic effects on absorption spectra for platinum complexes with light-activated activity against cancer cells**
J. Creutzberg, E. D. Hedegård
Physical Chemistry Chemical Physics, 2020, 22(46), pp. 27013-27023

ii **Polarizable embedding complex polarization propagator in a four- and two-component frameworks**
J. Creutzberg, E. D. Hedegård
Journal of Chemical Theory and Computation 2022, 18(6), pp. 3671-3686

iii **New relativistic quantum chemical methods for understanding light-induced therapeutics**
J. Creutzberg, E. D. Hedegård
Dalton Transactions 2022, 51(42), pp. 16055-16064

iv **A method to capture the large relativistic and solvent effects on UV-vis spectra of photo-activated metal complexes**
J. Creutzberg, E. D. Hedegård
Manuscript submitted to Physical Chemistry Chemical Physics

v **Electronic Circular Dichroism at the level of four-component Kohn–Sham density functional theory**
J. Creutzberg, E. D. Hedegård, O. Falklöf, T. Saue, P. Norman
Manuscript

vi **A method to explore the combined impact of relativistic and solvent effects on electronic circular dichroism spectra**
J. Creutzberg, E. D. Hedegård
Manuscript

All papers are reproduced with permission of their respective publishers.

Publications not included in this thesis

vii **OpenMolcas: From Source Code to Insight**

I. Fdez. Galván et al.
Journal of Chemical Theory and Computation 2019, 15(11), pp. 5925-5964

viii **The role of the active site tyrosine in the mechanism of lytic polysaccharide monooxygenase**
A. McEvoy, J. Creutzberg, R. K. Singh, M. J. Bjerrum, E. D. Hedegård
Chemical Science 2021, 12(1), pp. 352-362

Acknowledgements

It has been around four eventful years since I first arrived in Lund. Since then, I have managed to learn a lot and gained new friends and experiences in the process. While I stand as the sole author of this thesis, it could not have been achieved without the support of others. First and foremost, I would like to thank my supervisor Erik Hedegård. You have been both an excellent supervisor and a good friend. Without you, this thesis would not have been possible. I would also like to thank Ulf Ryde, my co-supervisor, who has provided me with the opportunity to consistently learn and discuss new science in our weekly journal clubs.

I would like to thank my colleagues in the theoretical chemistry division, both former and present. To Justin, I have always been able to count on you, whether it concerns work, cooking, going to the gym or if I just needed someone to talk to. Ernst, with you I have had the most interesting conversations concerning science, politics or life in general. Additionally, for teaching me about the ways of multi-configurational quantum chemistry. Samuel, you are just fun to be around and you always manage to bring a smile to my face. Thank you, Iria, Magne, Vilhelm, Kristoffer, Victor, Eric, Mona, Amanda and the people who are no longer active PhD students. You have all made the workplace a great environment to be in with all the fika and lunches.

To my parents, Anna and Lars and my brother Mattias, for always being there for me and believing in me.

Finally, I would like to thank Eline for all your support. I am grateful to have you in my life.

Populärvetenskaplig sammanfattning på svenska

Växelverkan mellan ljus och materia är ett fascinerande fält inom naturvetenskapen, där olika discipliner möts och samverkar för att att förstå en uppsjö av olika fysikaliska fenomen. Ett av dessa fenomen är hur ämnen tar upp ljus av specifika våglängder, vilket kallas för absorption, och kan enbart förklaras utifrån ett kvantmekaniskt perspektiv av verkligheten. Experiment där den här typen av interaktioner studeras kallas för spektrokskopi och är ett användbart verktyg för att få en detaljrik inblick i den elektroniska strukturen hos olika ämnen och kan exempelvis användas för att studera reaktioner. Att dra slutsatser utifrån spektran kan dock vara synnerligen svårt på grund av deras komplexitet, således behövs teoretiska modeller för att kunna förklara och tolka empiriska resultat. Detta görs genom att ekvationer inom teorin översätts till datormodeller, från vilka beräkningar av molekylära egenskaper sedan kan utföras.

I denna avhandling studeras molekylers ljusabsorption genom metoder inom kvantkemi. Primärt används täthetsfunktionalteori i kombination med linjär responsteori. Det senare är en form av tidsberoende störningsteori och bygger upp ett ramverk som kan användas för att bestämma både statiska och dynamiska molekylära egenskaper. Den egenskap av intresse är som ovan nämnts absorption, vilken återfås genom att vi bestämmer den eletriska dipolpolariserbarhetstensorn, som är en linjär responsfunktion. Från responsfunktionerna återfås sedan intensiteter och energier för excitationer i ett spektra.

För tyngre grundämnen i det periodiska systemet så räcker det inte längre med en enbart kvantmekanisk beskrivning, utan vi behöver inkludera Einsteins speciella relativitetsteori. Anledningen till detta är att elektroner nära kärnan känner av en mycket större potential i tyngre grundämnen och därmed har en högre genomsnittlig kinetisk energi. Utöver detta tillkommer att kopplingen mellan elektronens banrörelsemängdsmoment och spinn ger upphov till fler kvantiserade energinivåer. Både dessa fenomen kan ge upphov till en markant ändring för molekylorbitalerna, och behövs därmed för att ge en korrekt beskrivning av spektran. Ett exempel på ett viktigt sådant fall återfinns i studierna för platinkomplex som ingår i denna avhandling och som kan användas i cancerbehandling. Dessa komplex har en fördel gentemot andra platinkomplex, då de kan intas i en form som är oskadlig för kroppen. De aktiveras sedan specifikt i de områden av kroppen där cancervävnaden återfinns med hjälp av ljus, som framkallar en kemisk process som transformerar dem till en skadlig variant. Det är därmed av stor vikt att förstå vid vilka våglängder den här ljusframkallade aktiveringen kan ske, och studierna visar den påverkan som relativistiska effekter har på dessa.

Kemiska system är ofta såpass stora och komplexa att kvantkemiska metoder inte längre räcker till, exempelvis för proteiner. Ett sätt att kringgå detta problem är att dela in systemet i en del som är mer känslig (eller är av större intresse) som sedan behandlas med kvantkemiska metoder, och en mindre känslig del av systemet (omgivningen) som behandlas med metoder inom molekylmekanik. Vad som återstår är sedan att beskriva kopplingen mellan dessa två delsystem. Den metod som används inom denna avhandling går ut på att den kvantmekaniska delen känner av den elektrostatiska potentialen från omgivningen och den kvantmekaniska delen polariserar i sin tur omgivningen. På detta vis kan vi ta hänsyn till hur förändringar kopplade till ett visst delsystem påverkar det andra delsystemet.

Syftet med denna avhandling är att utveckla metoder som kombinerar relativistiska effekter och linjär responsteori med den ovan beskrivna metodiken att dela in ett kemiskt system i en kvantmekanisk och molekylmekanisk del. Dessa möjliggör studier av spektran för större och mer komplexa system med grundämnen från alla delar av det periodiska systemet.

Extending relativistic linear response theory to address solvent effects

Chapter 1

Light-activated anti-cancer platinum complexes

Several of the papers included in this thesis will involve heavy metal complexes used in cancer treatment. Historically, the treatment of cancer with transition metal complexes has been known since the 1970s, when *cis*-$[PtCl_2(NH_3)_2]$ (*cis*-Platinum) was first deployed[1]. Since then, other types of complexes have been approved worldwide, with a multitude more under development[2]. Yet, cancer treatment has long been associated with severe side effects[3]. The reason for these side effects is that *cis*-Pt and related complexes are labile, and thus complexes that are stable until activated may be able to remedy these side effects. Different types of activation mechanisms have been explored[2,4]. Here, successful candidates include transition metal complexes with a light-activated mechanism. Two types of activation mechanisms exist: The first is known as photodynamic therapy (PDT) and the second as photo-activated chemotherapy (PACT)[5]. The former employ complexes as photo-sensitizers in a process that results in the generation of singlet oxygen and oxygen radicals, whereas the latter, PACT, employ complexes that are decomposed upon irradiation with light. If the activation occurs inside the cancer cell, the singlet oxygen/radicals or the decomposed complex can attack DNA or proteins inside the cell, leading to cell death. An advantage of PDT is that the complexes (photo-sensitizers) can be recycled, while the advantage with the complexes used in PACT, is that they can be deployed and activated under hypoxic conditions often found in tumours.

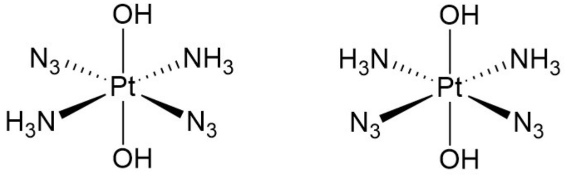

trans-Pt

cis-Pt

Figure 1.1: Lewis structures of *trans-trans-trans*-[Pt(N_3)$_2$(OH)$_2$(NH_3)$_2$] (*trans*-Pt) and *cis-trans-cis*-[Pt(N_3)$_2$(OH)$_2$(NH_3)$_2$] (*cis*-Pt) investigated in this thesis (taken from reference 6).

In this thesis (Paper I, II, and IV), we investigate two complexes with application in PACT: *trans-trans-trans*-[Pt(N_3)$_2$(OH)$_2$(NH_3)$_2$] (denoted *trans*-Pt) and *cis-trans-cis*-[Pt(N_3)$_2$(OH)$_2$(NH_3)$_2$] (denoted *cis*-Pt) (see Figure 1.1). Both display anti-cancer potency, and have been studied experimentally (in vitro) and computationally[7,8,9,10]. They are both octahedral complexes with a Pt(IV) centre in a low-spin d^6 configuration. This configuration is known to lead to kinetically inert molecules. This is in contrast to traditional complexes (like *cis*-[$PtCl_2(NH_3)_2$]), that have square planar symmetry with a Pt(II) centre and a d^8 configuration. Previous experimental studies have shown that they decompose when exposed to light under ambient conditions. The decomposition pathway is complex and varies depending on the solvent. In phosphate-buffered saline solutions, it has been shown that the azide ligands dissociate but that no reduction of the Platinum atom occurs. Moreover, they also found evidence that NH_3 is released[7,11]. For acidic aqueous solvents, however, the studies showed a release of N_3 , with an associated reduction of the metal center from Pt(IV) to Pt(II)[7,9]. The computational studies have confirmed the experiment and provided additional insights concerning the photo-activated decomposition pathways. They have shown that that light-absorption is associated with ligand-to-metal charge-transfer (LMCT) excitation from either the OH^- or N_3^- ligands to the Platinum atom[10,12]. A detailed analysis of the orbitals in the excitations shows that the accepting d-orbital on the Platinum atom is anti-bonding with respect to the ligands, and thus the population of it naturally favours dissociation. They also have shown that both singlet and triplet excited state favour the dissociation of ligands. While the singlet excited states are reached through vertical excitations, the triplet state has been shown to be populated through intersystem crossing .

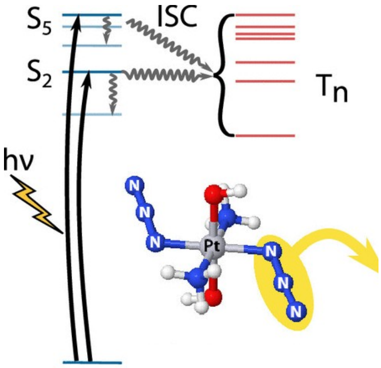

Figure 1.2: Schematic illustration of the Photo-activation of the *trans-trans-trans*-[Pt$(N_3)_2(OH)_2(NH_3)_2$] complex (Taken from reference [13], usage allowed under Creative commons)

Relativistic effects are anticipated to be important for the complexes, and have been accounted for to a certain degree by effective-core potentials (ECPs) [10,12] or a scalar-relativistic Douglas–Kroll–Hess Hamiltonian [13]. Moreover, since the complexes are always applied in an aqueous environment, solvent effects are considered to be important, and have been modelled implicitly through the conductor-like polarizable continuum model (CPCM) [12]. However, surprisingly, no rigorous treatment of either relativistic effects or that of a solvent has been done previously. This has partly been due to the lack of methods that can carry out this task. In this thesis, we, therefore, aim to systematically investigate the effect of a relativistic treatment on the absorption spectrum of the complexes in Figure 1.1. Moreover, we will develop a method that allows us to accurately account for the solvent effect, including both dynamics and the electronic effect of the solvent. We will account for relativistic effects either through the use of a four-component (4c) or two-component (X2C) wave function (see more in chapter 2). This will provide a rigorous treatment of spin-orbit coupling which is crucial for an accurate description of the excited states. Furthermore, an explicit solvent will be included through the use of the polarizable embedding model (see chapter 3).

Chapter 2

Electronic structure theory

A brief summary of electronic structure theory is given in this chapter, starting with an introduction to second quantization, which we use in most parts of this thesis. In section 2.2 we introduce the time-independent Schrödinger equation and the Born-Oppenheimer approximation. We then introduce a relativistic treatment of quantum mechanics through the Dirac equation. The next section describes Hartree-Fock theory before finally going into density functional theory. Most of the theory on second quantization and Hartree-Fock theory is based on the book by Helgaker and co-workers[14], while the relativistic parts are based on the review by Saue[15]. The DFT section is based on the book by Jensen[16] and the paper by Saue et. al[17]. We assume a closed-shell formalism for Hartree-Fock and DFT and that all equations make use of Hartree units.

2.1 Second quantization

A state in second quantization can be formulated as a so-called occupation number vector, containing an index k_p of either 1 for occupied and 0 for unoccupied orbitals

$$|\mathbf{k}\rangle = |k_1, k_2, ...k_M\rangle. \tag{2.1}$$

We thereafter define *annihilation operators*, $\hat{a}_p$ and their hermitian adjoint *creation operators*, $\hat{a}_p^\dagger$, whose operations on $|\mathbf{k}\rangle$ results in an electron being either *annihilated* or *created* from orbital p

$$\hat{a}_p|k_1, k_2, ...1_p...k_M\rangle = \Gamma_p^k|k_1, k_2, ...0_p...k_M\rangle \tag{2.2}$$

$$\hat{a}_p^\dagger|k_1, k_2, ...0_p...k_M\rangle = \Gamma_p^k|k_1, k_2, ...1_p...k_M\rangle. \tag{2.3}$$

The Γ represents a phase factor being either -1 or 1 depending on whether the number of orbitals standing before p is even or odd. A combination of these operators that contains the same number of creation and annihilation operators conserve the number of electrons and are called *excitation operators*, $a_p^\dagger a_q$. Using excitation operators, we can express any one-electron or two-electron operator in second quantization and this will be done in the following sections.

2.2 The molecular Schrödinger equation

The time-independent molecular Schrödinger equation is the eigenvalue equation,

$$\hat{H}\Psi = E\Psi, \tag{2.4}$$

with the eigenvalue E being the discrete energy levels of the system of interest, the wave function Ψ being the eigenstate, and $\hat{H}$ is the Hamiltonian. In first quantization, the Hamiltonian is given

$$\hat{H} = -\sum_A^M \frac{1}{2M_A}\nabla_A^2 + \hat{H}_e + \hat{H}_{mp}. \tag{2.5}$$

The first term accounts for the kinetic energy of the nuclei, whereas the last term is the mass-polarization term. The $\hat{H}_e$ collects all degrees of freedom for the electronic part as well as the nuclear repulsion

$$\hat{H}_e = -\frac{1}{2}\sum_i \nabla_i^2 - \sum_i \frac{Z_A}{r_{Ai}} + \sum_i \sum_{j>i} \frac{1}{r_{ij}} + \sum_A \sum_{B>A} \frac{Z_A Z_B}{r_{AB}}, \tag{2.6}$$

where the subscripts A and B refer to the nuclei, and the subscripts i and j refer to the individual electrons. Moreover, we have assumed atomic units. The first two terms describe the kinetic energy of the electrons and nuclear-electron attraction, whereas the last two terms describe the electron and nuclear repulsion. In the following we will work within the Born-Oppenheimer approximation, i.e., we use a product wave function where the wave function can be expanded in a basis of electronic functions

$$\Psi(R, r) = \sum_n C_n(R)\Psi_e(R, r), \tag{2.7}$$

where the nuclear wave functions are the expansion coefficients $\{C_n\}$, and R and r refer to the nuclear and electronic coordinates. By assuming no coupling between the nuclear coordinates and the electronic wave function (and also neglecting the mass-polarization term) we can separate 2.4 into an electronic and a nuclear part, and only solve the electronic part

$$\hat{H}_e \Psi_e = E_e \Psi_e. \tag{2.8}$$

Moving to a second quantization formalism, the Hamiltonian is given as

$$\hat{H}_e = \sum_{pq} h_{pq} a_p^\dagger a_q + \frac{1}{2} \sum_{pqrs} g_{pqrs} a_p^\dagger a_r^\dagger a_s a_q + h_{nuc}, \tag{2.9}$$

where h_{nuc} is the nuclear-nuclear repulsion and h_{pq}, g_{pqrs} are integrals defined as

$$h_{pq} = \int \psi_p^*(\boldsymbol{x_1}) \Big(-\frac{1}{2}\nabla^2 - \sum_A \frac{Z_A}{r_{A_1}} \Big) \psi_q(\boldsymbol{x_1}) d\boldsymbol{x_1} \tag{2.10}$$

$$g_{pqrs} = \int \int \frac{\psi_p^*(\boldsymbol{x_1}) \psi_r^*(\boldsymbol{x_2}) \psi_q(\boldsymbol{x_1}) \psi_s(\boldsymbol{x_2})}{r_{12}} d\boldsymbol{x_1} d\boldsymbol{x_2}. \tag{2.11}$$

where $\{\psi_p\}$ are basis functions used to expand Ψ_e, and $\boldsymbol{x}$ are the coordinates with both a spin and spatial part. We have here and in the following denoted indices of occupied orbitals i, j and unoccupied orbitals a, b. General orbitals are denoted with index p, q.

2.3 The Dirac equation

When velocities close to the speed of light are involved, we need to consider relativistic effects. For chemistry, this is mainly seen in heavy elements where the electrons near the nuclei can approach the speed of light. The inclusion of these effects into the mathematical framework of quantum mechanics entails a transformation of the operators. After carrying out these transformations, we obtain the relativistic counterpart of the Schrödinger equation called the Dirac equation. The changes do not affect the Born-Oppenheimer approximation Thus, we can define an electronic Hamiltonian in a similar fashion. The one-electron operator can be defined as

$$\hat{h} = \sqrt{m^2c^4 + c^2 \Big(\hat{\mathbf{p}} + e\mathbf{A}(r,t) \Big)^2} - e\phi(r,t) \tag{2.12}$$

where m is the mass of the electron and the field is introduced with the principle of minimal coupling[15,18] with scalar potential $\phi(r,t)$ and vector potential $\mathbf{A}(r,t)$.

With a static external potential $V_{\text{ext}} = -e\phi(r,t)$ (representing the nuclear-electron attraction) and $\mathbf{A}(r,t) = 0$ (Coulomb gauge), the one-electron operator becomes

$$\hat{h} = \hat{h}_D + \hat{V}_{\text{ext}} = \begin{pmatrix} \mathbf{0}_2 & c(\boldsymbol{\sigma}\cdot\hat{\mathbf{p}}) \\ c(\boldsymbol{\sigma}\cdot\hat{\mathbf{p}}) & -2c^2\mathbf{I}_2 \end{pmatrix} + \begin{pmatrix} V_{\text{ext}}\mathbf{I}_2 & \mathbf{0}_2 \\ \mathbf{0}_2 & V_{\text{ext}}\mathbf{I}_2 \end{pmatrix}, \tag{2.13}$$

where the unit matrix $\mathbf{I}_2$ and the Pauli matrices $\boldsymbol{\sigma}$ have been defined, each representing a 2x2 matrix. The Pauli matrices are given as:

$$\sigma_1 = \begin{pmatrix} 0 & 1 \\ 1 & 0 \end{pmatrix}, \sigma_2 = \begin{pmatrix} 0 & -i \\ i & 0 \end{pmatrix}, \sigma_3 = \begin{pmatrix} 1 & 0 \\ 0 & -1 \end{pmatrix}. \tag{2.14}$$

The main difference to the non-relativistic case is the relativistic expression of the momentum, which instead of a scalar equation now involves matrices. Due to this change, the wave function is now comprised of large and small component parts, respectively, which themselves are two-component wave functions (comprised of different spin parts):

$$|\Psi\rangle = \begin{pmatrix} \psi^L \\ \psi^S \end{pmatrix} \qquad\qquad |\psi^X\rangle = \begin{pmatrix} \psi^X_\alpha \\ \psi^X_\beta \end{pmatrix}. \tag{2.15}$$

The electron-electron interaction in relativistic quantum mechanics is complicated, and a closed form does not exist. Therefore, the electron-electron interaction is expressed as a perturbation expansion in terms of $1/c$. From this expansion, we can identify the zeroth order term as the instantaneous Coulomb interaction, which is expressed similarly to non-relativistic theory

$$\hat{g}^{Coulomb}(1,2) = \frac{\mathbf{I}_4 \cdot \mathbf{I}_4}{r_{12}}, \tag{2.16}$$

with I_4 being the identity (4x4). Higher order terms include the Breit term, which in turn can be divided into the Gaunt and gauge terms. For most applications, however, the Coulomb part is sufficient, and we will therefore use this approximation in this thesis. The corresponding Hamiltonian is called the Dirac-Coulomb Hamiltonian. The Dirac-Coulomb Hamiltonian is identical to Eq. 2.9, but the one-electron integrals h_{pq} in Eq. 2.10 are replaced with integrals over $\hat{h}_D$ in Eq. 2.13.

Qualitatively the changes due to the relativistic effects are in atoms a contraction of the s and p orbitals which lead to an increase in the screening of the nuclear charge that in turn leads to an expansion of the d and f orbitals. These effects are called *scalar-relativistic*. Furthermore, the degenerate orbitals will split due to the spin-orbit coupling and is essential in describing, e.g., L-edge core-spectroscopy.

We have now established the basic aspects of relativistic quantum chemistry. Most of the methods that follow will have the same structure, regardless of being relativistic or not. Nevertheless, there will be differences. In the following sections, we will therefore point out when these occur.

2.4 Hartree-Fock theory

2.4.1 Slater determinants

Although we now only consider the electronic wave function, we still need to define a form that allows us to describe N-electron systems. For this purpose, we define a so-called Slater determinant.

$$\Psi(1,2...N) = \frac{1}{\sqrt{N!}} \begin{vmatrix} \phi_1(1) & \dots & \phi_N(1) \\ \vdots & \ddots & \vdots \\ \phi_1(N) & \dots & \phi_N(N) \end{vmatrix}. \tag{2.17}$$

This choice of wave function is both anti-symmetric concerning permutation of any pair of electrons (and thereby fulfils the Pauli principle) and is additionally a product wave function, making it suitable for N-electron systems.

The spin-orbitals are unchanged over columns and the electron coordinate (represented by a number) is unchanged over rows. In second quantization, any Slater-determinant can be expressed as a sequence of creation operators acting on the vacuum state $|vac\rangle$, which is the state in which none of the orbitals are occupied

$$\Psi(1,2...N) = \left(\prod_i a^\dagger_{i\alpha} a^\dagger_{i\beta}\right)|vac\rangle. \tag{2.18}$$

2.4.2 Hartree-Fock equations

In Hartree-Fock theory, we impose a variational condition on a trial Slater determinant wave function. We define such a trial wave function as the state

$$|\tilde{0}\rangle = e^{-\hat{\kappa}}|0\rangle \tag{2.19}$$

where κ is the orbital rotation parameter, defined as

$$\hat{\kappa} = \sum_{pq} \kappa_{pq} \hat{a}^\dagger_p \hat{a}_q \tag{2.20}$$

where κ_{pq} are the variational parameters. We return to its definition in a time-dependent form in a later chapter. For now, it is sufficient to note that by defining an energy expression for the trial wave function, employing a Baker-Campbell Hausdorff expansion on this expression and requiring the gradient with respect to κ_{ai} to vanish, we obtain a variational condition

$$f_{ia} = \langle 0|[\hat{f}, \hat{a}_i^\dagger \hat{a}_a]|0\rangle \tag{2.21}$$

for elements f_{ai} of the so-called Fock matrix, $\mathbf{f}$. The corresponding Fock operator reads

$$\hat{f} = \sum_{pq} f_{pq}\hat{a}_p^\dagger \hat{a}_q = \sum_{pq}\Big(h_{pq} + \sum_i \big(2g_{pqii} - g_{piiq}\big)\Big)\hat{a}_p^\dagger \hat{a}_q. \tag{2.22}$$

where the expression for the one- and two-electron integrals are given in equations 2.10-2.11. It can be noted that the Fock operator includes the molecular orbitals we are trying to optimize, which means that solving the HF equations requires an iterative procedure known as a *self-consistent field* method.

For practical calculations on molecular systems, we generally expand the molecular orbitals ϕ in terms of the atomic orbitals AO χ

$$\phi_p = \sum_\mu \chi_\mu C_{\mu p}. \tag{2.23}$$

Inserting this expansion into the Hartree-Fock equations leads to the *Roothan–Hall* equations (here in matrix form)

$$\mathbf{f}^{AO}\mathbf{C} = \mathbf{S}\mathbf{C}\boldsymbol{\epsilon}, \tag{2.24}$$

where $\mathbf{S}$ is the overlap matrix and $\mathbf{C}$ is a vector containing the molecular orbital coefficients.
In a four-component framework, the MOs will be expressed in terms of vectors comprised of both large and small component basis functions

$$|\phi_i\rangle = \sum_\kappa^{N_L} \begin{pmatrix} |\chi_\kappa^L\rangle \\ 0 \end{pmatrix} C_\kappa^L + \sum_\lambda^{N_s} \begin{pmatrix} 0 \\ |\chi_\lambda^S\rangle \end{pmatrix} C_\lambda^S. \tag{2.25}$$

The large and small component of the wave function will have separate expansion coefficients. This leads to the Fock matrix having four different blocks with respect to the large and small components

$$\mathbf{F} = \begin{pmatrix} \mathbf{F}^{LL} & \mathbf{F}^{LS} \\ \mathbf{F}^{SL} & \mathbf{F}^{SS} \end{pmatrix}. \tag{2.26}$$

Compared to a non-relativistic model, where only $\mathbf{F}^{LL}$ is relevant, the additional presence of $|\chi^S\rangle$ causes the number of integrals to increase. Since this increase is due to the small component, a class of methods where only the large component is accounted for has been constructed, and they reduce the computational effort significantly. These methods are denoted as two-component methods.

2.5 Kohn-Sham density functional theory

Hartree-Fock theory has a flaw in that it treats electron-electron interactions in an average fashion, i.e., it misses the so-called correlation energy. In this section, we present Kohn-Sham density functional theory which is a variant of DFT that introduces an orbital approximation through a single Slater determinant, similar to HF theory. Unlike HF theory, however, it also includes electron correlation[16]. Kohn-Sham DFT builds on the Hohenberg-Kohn theorems, stating that the electron density, ρ, for the ground state of a system is uniquely defined. Thus, from the electron density, we may obtain the ground state energy by a variational procedure. The energy functional $E[\rho]$ can be defined as

$$E[\rho] = T_s[\rho] + V^{ext}[\rho] + J[\rho] + E_{NN} + E_{xc}[\rho]. \tag{2.27}$$

Where the first term is the kinetic energy of the electrons in a fictitious system with non-interacting electrons

$$T_s[\rho] = \sum_i \langle\phi_i| - \frac{1}{2}\nabla^2|\phi_i\rangle, \tag{2.28}$$

the second term is the external potential for the nuclear-attraction potential

$$V^{ext}[\rho] = \sum_A \int \frac{Z_A}{|r - R_A|}\rho(r)dr, \tag{2.29}$$

and the third term represents the electron-electron interaction

$$J[\rho] = \frac{1}{2}\int\int \frac{\rho(r_1)\rho(r_2)}{r_{12}}dr_1dr_2. \tag{2.30}$$

The fourth term E_{NN} models the nuclear-nuclear repulsion, which due to the Born-Oppenheimer approximation can be added as a constant to the energy functional. The fifth term represents the exchange-correlation energy, and this takes into account the exchange part which is not explicitly included as in Hartree-Fock. Additionally, it contains a correlation part. This part is in practice defined through a parametric expression and can be done in many different ways, giving rise to many different classes of DFT functionals. We would also like to add that relativistic extensions of the Hohenberg-Kohn theorems exist[19], thereby enabling the use of four component DFT. Since we assume a Dirac-Coulomb Hamiltonian, the resulting relativistic changes in the expressions for the energy functional are small and are mainly reflected in the first term of Eq. 2.27, which due to the changed expression for the kinetic energy operator assumes the form

$$T_s[\rho] = \sum_i \langle \phi_i | \hat{h}_D | \phi_i \rangle. \tag{2.31}$$

2.5.1 KS-DFT in second quantization

The KS-DFT wave function ansatz is defined analogously to HF[17], with the parameterized wave function being the same as in 2.19. Through this, the electron density can be defined as

$$\rho(r, \kappa) = \sum_{pq} \tilde{D}_{pq}(\kappa) \Omega_{pq}(r), \tag{2.32}$$

where $\tilde{D}_{pq}$ is the density matrix and $\Omega_{pq}(r)$ is the overlap distribution:

$$\tilde{D}_{pq} = \langle \tilde{0} | \hat{a}_p^\dagger \hat{a}_q | \tilde{0} \rangle \qquad \Omega_{pq}(r) = \phi_p^\dagger(r) \phi_q(r). \tag{2.33}$$

This leads to the definition of the KS energy expression in second quantization[17]

$$E[\rho(\kappa)] = \sum_{pq} h_{pq} \tilde{D}_{pq} + \frac{1}{2} \sum_{pqrs} g_{pqrs} \tilde{D}_{pq} \tilde{D}_{rs} + E_{xc}[\rho(\kappa)] + V_{NN} \tag{2.34}$$

The variational minimization will lead to an expression very similar to equation 2.24.

2.5.2 Exchange-correlation functionals

We mentioned above that the exchange-correlation part can be defined in various ways. We will here introduce the three most common types of exchange functionals. In the local density approximation (LDA) we can define the exchange-correlation energy as an integral over the energy density e_{xc}, which is a functional of the electron density

$$E_{xc}^{LDA}[\rho(\kappa)] = \int e_{xc}\big(\rho(r, \kappa)\big) dr. \tag{2.35}$$

Usually, however, this method yields results with poor accuracy for atoms and molecules. A more advanced form exists in the generalized gradient approximation (GGA)

$$E_{xc}^{GGA}[\rho(\kappa)] = \int e_{xc}\big(\rho(r, \kappa), \xi(r, \kappa)\big) dr. \tag{2.36}$$

where the exchange-correlation density is also dependent on the norm of the gradient of the density $\xi(r,\kappa)$. Moreover, there are hybdrid functionals in which part of the exchange is incorporated through the Hartree-Fock method

$$E_{xc}^{hybrid}[\rho(\kappa)] = E_{xc}^{GGA}[\rho(\kappa)] + \gamma E_{x}^{HF}[\rho(\kappa)], \tag{2.37}$$

where γ is the amount of Hartree-Fock exchange used.
Yet another class of functionals exist: the so-called long-range corrected functionals. They correct for the wrong asymptotic behaviour of the electron-electron interaction in standard functionals. They do so by splitting the Coulomb operator into two parts, describing the short and long-range interactions

$$\frac{1}{r_{12}} = \frac{1-[\alpha+\beta erf(\mu r_{12})]}{r_{12}} + \frac{\alpha+\beta erf(\mu r_{12})}{r_{12}}. \tag{2.38}$$

In the expression, α, β and μ are parameters and erf is the error function. These functionals are essential for obtaining an accurate description of charge-transfer states and ionization potentials[20], and are well suited for Time-dependent density functional theory (TD-DFT) which has been extensively applied in this thesis.

Chapter 3

Polarizable embedding

To allow a description of systems where larger environments are important, QM methods have been combined with computationally efficient molecular mechanics (MM) methods, dividing the entire system into QM and MM regions (see Figure 3.1); this is commonly known as QM/MM[21,22,23]. In this chapter, we introduce QM/MM with a polarizable MM part, which is especially important to consider in excitation processes.

3.1 QM/MM with electrostatic and polarizable embedding

Various QM/MM schemes exist but we here only focus on the so-called additive variant, where the energy of the total system is given as

$$E_{tot} = E_{QM} + E_{env} = E_{QM} + E_{MM} + E_{QM/MM}. \tag{3.1}$$

As seen from Eq. 3.1, the total energy is comprised of the energy of the quantum part (E_{QM}), the energy of all interactions with the MM part (E_{MM}) and a coupling term ($E_{QM/MM}$) which contains the contributions

$$E_{QM/MM} = E_{es} + E_{ind} + E_{non-el} + E_{bond}. \tag{3.2}$$

The first two terms have expressions known from classical electrostatics where E_{es}, is the electrostatic interaction between the QM system and the environment, while E_{ind} accounts for the mutual polarization between the environment and the QM system. The third term, E_{non-el}, accounts for all non-bonded interactions that are not included in the first two terms, e.g., exchange repulsion or dispersion. The last term,

E_{bond} is only relevant if there are covalent bonds between QM and MM systems. We will here work with a polarizable QM/MM scheme[24,25,26,27], denoted the *polarizable embedding* (PE) model[28,29]. The PE model entails a description of E_{el} through electric multipoles while E_{ind} is described through point polarizabilities. Both the electric multipoles and the point-polarizabilities are obtained by fragmentation of the environment followed by QM calculations on the individual fragments (see Figure 3.2). In the two subsections below, the explicit forms of E_{es} and E_{ind} will be elaborated.

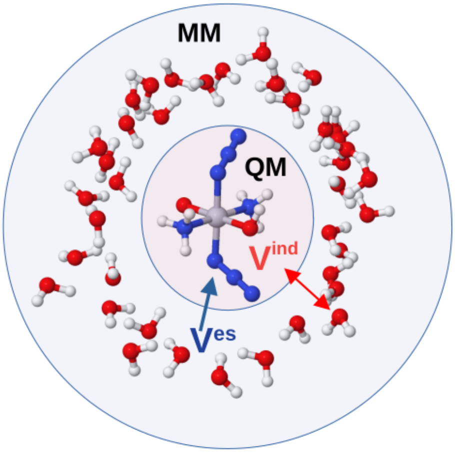

Figure 3.1: Illustration of the subdivision of a system into regions in QM/MM.

3.1.1 Electrostatic interactions with multipole expansions

The description of electrostatics in polarizable embedding models generally builds on multipole expansions. We take the outset in the potential $V(\mathbf{r})$ inside the QM region, due to the environment density $\rho_i(\mathbf{r})$ for fragment i. From a Taylor expansion of $(\mathbf{r}-\mathbf{R}_i)^{-1}$, we obtain the following potential

$$V(\mathbf{r}) = \frac{q_i}{|\mathbf{r}-\mathbf{R}_i|} - \sum_{\alpha} \mu_{i,\alpha}\left(\frac{\partial}{\partial r_\alpha}\frac{1}{|\mathbf{r}-\mathbf{R}_i|}\right) + \frac{1}{2}\sum_{\alpha,\beta} Q_{i,\alpha\beta}\left(\frac{\partial^2}{\partial r_\alpha \partial r_\beta}\frac{1}{|\mathbf{r}-\mathbf{R}_i|}\right) + \cdots, \tag{3.3}$$

where we have defined the cartesian components ($\alpha, \beta = x, y, z$) of the charge, dipole and quadrupole moments (q_i, $\mu_{i,\alpha}$ and $Q_{i,\alpha\beta}$), respectively. Examples of the first two are given below

$$q_i = \int \rho_i(\mathbf{r})\mathrm{d}\mathbf{r}, \qquad \mu_{i,\alpha} = \int (r_\alpha - R_{i,\alpha})\rho_i(\mathbf{r})\mathrm{d}\mathbf{r}. \tag{3.4}$$

To use Eq. 3.4 in our PE model, it is exploited that the Taylor expansion in equations 3.3 converges faster if the multipoles are distributed, rather than have one common origin[30]. Therefore, each fragment is further split up into sites s. The sites coincide with atoms within the individual fragments and atom-centred multipoles are obtained with the LoProp method[31], which requires a QM calculation for each fragment.

For a more compact notation, we introduce the multi-index notation where the derivatives in equation 3.3 are written[32]

$$\nabla^k \equiv \frac{\partial^{|k|}}{\partial \mathbf{r}^k} = \frac{\partial^{k_x+k_y+k_z}}{\partial x^{k_x}\partial y^{k_y}\partial z^{k_z}}, \tag{3.5}$$

using a multi-index $k = (k_x, k_y, k_z)$ to define both Cartesian component(s) and order of expansion. Likewise, a vector is defined $\mathbf{r}^k = r_x^{k_x} r_y^{k_y} r_z^{k_z}$. With this nomenclature, the Taylor expansion that led to equation 3.3 is for site s

$$\frac{1}{|\mathbf{r}-\mathbf{r}_s|} = \sum_{|k|=0}^{\infty}\sum_{k\in|k|}\frac{(-1)^{|k|}}{k!}\Big(\nabla^k\frac{1}{|\mathbf{r}-\mathbf{r}_s|}(\mathbf{r}-\mathbf{r}_s)^k\Big), \tag{3.6}$$

where the sum according to the definition of the multi-index is over $3^{|k|}$ elements. By introducing interaction operators[30] $T_{ij}^{(k)} = \nabla_i^k|\mathbf{r}_i - \mathbf{R}_j|^{-1}$ or $T_j^{(k)} = \hat{\nabla}^k|\mathbf{r} - \mathbf{R}_j|^{-1}$ and a general nomenclature for the multipole moments, $M_s^{(k)}$, we can write the potential for the interaction between the MM and QM part in the compact form

$$\begin{aligned}\hat{V}^{es} &= \sum_s\sum_{|k|=0}\frac{(-1)^{|k|}}{k!}\Big(M_s^{(k)}\sum_{pq}\langle\phi_p|T_s^{(k)}|\phi_q\rangle\hat{a}_p^\dagger\hat{a}_q + M_s^{(k)}\sum_M Z_M T_{Ms}^{(k)}\Big)\\ &= \hat{V}^e + \hat{V}^{nuc},\end{aligned} \tag{3.7}$$

where the sum over all sites s has been introduced. The electronic part is often written

$$\hat{V}^e = \sum_s\sum_{|k|=0}\frac{(-1)^{|k|}}{k!}M_s^{(k)}\sum_{pq}t_{pq,s}^{(k)}\hat{a}_p^\dagger\hat{a}_q \qquad t_{pq,s}^{(k)} = -\langle\phi_p|T_s^{(k)}|\phi_q\rangle \tag{3.8}$$

where the integrals over $T_s^{(k)}$ is contained in $t_{pq,s}^{(k)}$. The resulting electrostatic energy, E_{es}, is thereafter obtained as the expectation value of $\hat{V}^{es}$

$$E_{es} = \langle 0|\hat{V}^{es}|0\rangle. \tag{3.9}$$

3.1.2 Induced dipole polarization

The electrostatic interaction between the MM and QM regions will polarize the QM density $\rho(\mathbf{r})$ and this polarization will automatically be included through the SCF procedure when the $\hat{V}^{es}$ operator is included in the Hamiltonian. However, the density $\rho_i(\mathbf{r})$ of any fragment i within the MM system will also be polarized by the combined field from the QM subsystem and all other fragments. In classical electrostatics, the polarization of $\rho_i(\mathbf{r})$ is associated with inducing a dipole (as well as higher order induced moments). We proceed as in the previous subsection by a Taylor expansion, this time of the dipole moment

$$\mu_{\alpha,i}(\boldsymbol{\mathcal{E}}) = \mu_{\alpha,i}(\mathbf{0}) + \mu_{\alpha,i}^{ind} = \mu_{\alpha,i}(\mathbf{0}) + \sum_{\beta} \frac{\partial \mu_{\alpha,i}}{\partial \mathcal{E}_\beta} \mathcal{E}_\beta + \cdots . \tag{3.10}$$

Truncating the expression at the linear term, the first term is the static dipole moment of fragment i, whereas the second is the polarizability tensor $\boldsymbol{\alpha}_i$ times the electric field $\boldsymbol{\mathcal{E}}$. Terminating the expansion at the linear term we have the induced dipole, with the associated energy expression

$$E_{ind,i}(\boldsymbol{\mathcal{E}}) = \sum_{\alpha} \mu_{\alpha,i}^{ind} \mathcal{E}_\alpha = -\frac{1}{2} \sum_{\alpha\beta} \mathcal{E}_\alpha \alpha_{\alpha\beta,i} \mathcal{E}_\beta = -\frac{1}{2} \boldsymbol{\mathcal{E}}^T \cdot (\boldsymbol{\alpha}_i \cdot \boldsymbol{\mathcal{E}}). \tag{3.11}$$

As in the previous section, each fragment in the environment is associated with a number of sites, containing site-polarizabilities (in addition to static multipoles), denoted $\boldsymbol{\alpha}_s$. The polarizabilities are also obtained with the LoProp method.[31] The field inducing a dipole on site s has contributions from QM electrons and nuclei as well as the multipoles, leaving the total field as

$$\hat{\boldsymbol{\mathcal{E}}}_s = \hat{\boldsymbol{\mathcal{E}}}_s^{el} + \boldsymbol{\mathcal{E}}_s^{nuc} + \boldsymbol{\mathcal{E}}_s^{es}, \tag{3.12}$$

and $\boldsymbol{\mu}^{ind}$ is now obtained according to equation 3.13

$$\boldsymbol{\mu}_s^{ind} = \boldsymbol{\alpha}_s \Big[\hat{\boldsymbol{\mathcal{E}}}_s - \sum_{s' \neq s} \boldsymbol{T}_{ss'}^{(2)} \boldsymbol{\mu}_{s'}^{ind} \Big], \tag{3.13}$$

where the last term describes the field induced due to the induced dipoles on all other sites. The electronic and nuclear fields are given as

$$\hat{\boldsymbol{\mathcal{E}}}_s^e = -\sum_{pq} t_{pq,s}^{(1)} \hat{a}_p^\dagger \hat{a}_q \qquad\qquad \boldsymbol{\mathcal{E}}_s^n = \sum_M Z_M T_{Ms}^{(1)}. \tag{3.14}$$

By modifying equation 3.13 and arranging the field- and induced dipole moment vectors in a vector of vectors, e.g., $\hat{\boldsymbol{\mathcal{E}}} = (\hat{\boldsymbol{\mathcal{E}}}_1, \ldots, \hat{\boldsymbol{\mathcal{E}}}_s, \ldots, \hat{\boldsymbol{\mathcal{E}}}_S)$ of length $3S$, we obtain a matrix equation[33] for the induced dipole moments

$$\boldsymbol{\mu}^{ind} = \mathbf{R} \cdot \hat{\boldsymbol{\mathcal{E}}}, \tag{3.15}$$

where we have defined the Relay matrix with inverse site-polarizabilities on the diagonal

$$\mathbf{R} = \begin{pmatrix} \boldsymbol{\alpha}_{11}^{-1} & \cdots & -\mathbf{T}_{1S}^{(2)} \\ \vdots & \ddots & \vdots \\ -\mathbf{T}_{S1}^{(2)} & \cdots & \boldsymbol{\alpha}_{SS}^{-1} \end{pmatrix}^{-1} . \tag{3.16}$$

Inserting 3.15 into Eq. 3.11 we then arrive at the final expression for the induced energy.

$$E_{ind} = -\frac{1}{2}\langle\, \hat{\boldsymbol{\mathcal{E}}}\,\rangle^T \mathbf{R} \langle\, \hat{\boldsymbol{\mathcal{E}}}\,\rangle \tag{3.17}$$

With outset in equations 3.9 and 3.17, the SCF equations from chapter 2 can be modified to include multipoles and polarizabilities in the environment by augmenting the Fock operator (cf. equation 2.22) with an effective environment operator, i.e.

$$\hat{f}^{tot} = \hat{f} + \hat{v}^{\mathrm{PE}} \tag{3.18}$$

with

$$\hat{v}^{\mathrm{PE}} = \hat{V}^{es} - \langle 0|\hat{\boldsymbol{\mathcal{E}}}|0\rangle^T \mathbf{R} \hat{\boldsymbol{\mathcal{E}}}^{e}. \tag{3.19}$$

Since we are mostly working within a four-component framework in this thesis, we note that the Fock operator in Eq. 3.18 will be represented on the block diagonal form as in Eq. 2.26. However, the blocks for the environment operator $\hat{v}_{\kappa\lambda}^{\mathrm{PE},XY} = \langle \chi_\kappa^X | \hat{v}^{\mathrm{PE}} | \chi_\lambda^Y \rangle$ only have non-zero contributions for the diagonal blocks (see reference[34]). This leads to the total Fock operator in Eq. 3.18 having the following manifestation in a four-component framework

$$\mathbf{F} = \begin{pmatrix} \mathbf{F}^{LL} + \mathbf{v}^{\mathrm{PE},LL} & \mathbf{F}^{LS} \\ \mathbf{F}^{SL} & \mathbf{F}^{SS} + \mathbf{v}^{\mathrm{PE},SS} \end{pmatrix} . \tag{3.20}$$

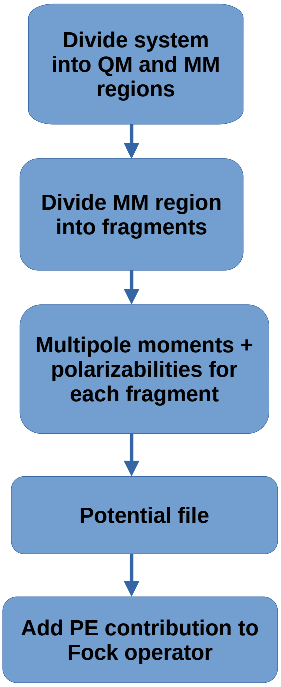
Divide system into QM and MM regions
Divide MM region into fragments
Multipole moments + polarizabilities for each fragment
Potential file
Add PE contribution to Fock operator

Figure 3.2: A flowchart describing the procedure to obtain a potential describing the environment

3.2 The LoProp method

The localized properties (LoProp)[31] approach provides an efficient and accurate way to calculate localized static properties. It relies on a localized orthonormal basis, that is constructed based on the overlap matrix by performing a step-wise orthonormalization procedure. Each step is carried out for the atomic blocks (A and B) and the occupied and virtual subspaces (o and v) of the overlap matrix. From the four subsequent transformation matrices, a final transformation matrix $\mathbf{T}$ is constructed. This transformation matrix is then used to transform the one-electron density matrix $\mathbf{D}$ (in the AO basis) and the property matrix $\mathbf{O}$ to the LoProp basis

$$\mathbf{D}^{\mathbf{LoProp}} = \mathbf{T}^{-1}\mathbf{D}\mathbf{T} \tag{3.21}$$

$$\mathbf{O}^{\mathbf{LoProp}} = \mathbf{T}^{-1}\mathbf{O}\mathbf{T} \tag{3.22}$$

From these relations, we can then obtain static properties such as charges and dipole moments that are localized. In addition to static local multipole moments, the method can also be used to obtain localized polarizabilities. The original implementation was only used to obtain static polarizabilities, and that is what it is used for in this thesis. However, we note that extensions to obtain frequency-dependent polarizabilities also exist[35,36,37].

Chapter 4

Linear response theory

Response theory is used to calculate static and frequency-dependent molecular properties, which in turn can be used to calculate various types of spectroscopy[38]. In this chapter, a brief overview of *linear* response theory is given. Higher-order response equations have been derived[39], but all papers included in this thesis stop at the linear order (which is sufficient to calculate, e.g., UV-vis and ECD spectra). While the first response theory formulations were done in the so-called Ehrenfest formulation[38], we here follow a later (and more general) quasi-energy formulation[17,39,40,41] and the chapter is written mainly with inspiration from papers by Christiansen *et al.*[40] and Helgaker *et al.*[39]

4.1 The quasi energy

Response theory is essentially a formulation of time-dependent perturbation theory where we seek to approximate the time-dependent Schödinger equation

$$\hat{H}|\bar{0}\rangle = i\frac{\partial}{\partial t}|\bar{0}\rangle \, . \tag{4.1}$$

The Hamiltonian can be divided into a time-independent part, $\hat{H}_0$, with known solutions and the electromagnetic field, $\hat{V}(t)$, as a time-dependent perturbation. Thus the Hamiltonian becomes

$$\hat{H} = \hat{H}_0 + \hat{V}(t). \tag{4.2}$$

The solutions to $\hat{H}_0$ can be obtained as described in chapter 2 while $\hat{V}(t)$ can be expressed as a series expansion of monochromatic, periodic perturbations

$$V(t) = \sum_k exp(-i\omega_k t) \sum_X \epsilon_X(\omega_k)\hat{X} \ . \tag{4.3}$$

In equation 4.3, $\hat{X}$ are property (perturbation) operators, ϵ_X their corresponding field strength parameters, and ω_k are the frequencies that the k'th perturbation oscillates with.

A general solution (wave function) to equation 4.1 can be expressed as

$$|\bar{0}\rangle = e^{-iF(t)}|\tilde{0}\rangle, \tag{4.4}$$

where $F(t)$ is a time-dependent phase factor and $|\tilde{0}\rangle$ is the phase-isolated part of the wave function. The time-evolution of a property with operator $\hat{X}$ can be given as the perturbation expansion

$$\langle\tilde{0}|\hat{X}|\tilde{0}\rangle = \langle 0|\hat{X}|0\rangle + \sum_k exp(-i\omega_k t)\sum_Y \langle\langle\hat{X};\hat{Y}\rangle\rangle_{\omega_k}\epsilon_Y(\omega_k) + \cdots \tag{4.5}$$

where $\langle\langle\hat{X};\hat{Y}\rangle\rangle_{\omega_k}$ are the linear response functions. A relation between the response function and $F(t)$ in equation 4.4 can be obtained from inserting equation 4.4 into equation 4.1, followed by projection with $\langle\tilde{0}|$, and isolating the time-derivative of $F(t)$

$$Q(t) \equiv \dot{F}(t) = \langle\tilde{0}|\big(\hat{H} - i\frac{\partial}{\partial t}\big)|\tilde{0}\rangle. \tag{4.6}$$

This quantity is also known as the quasi-energy, which (as will be apparent below) can be directly related to the response functions. In the time-independent limit, the quasi-energy reduces to the normal energy. Through the Hellman-Feynman theory, we can then identify static molecular properties (the first term in equation 4.5) as derivatives with respect to the energy. A time-dependent extension of the Hellman-Feynman theorem can be formulated for the quasi-energy as

$$\frac{dQ}{d\epsilon} = \langle\tilde{0}|\frac{\partial\hat{H}}{\partial\epsilon}|\tilde{0}\rangle - i\frac{\partial}{\partial t}\Big\langle\tilde{0}\Big|\frac{d\tilde{0}}{d\epsilon}\Big\rangle. \tag{4.7}$$

The identification of properties as derivatives with respect to the quasi-energy is not straightforward due to the second term. However, by time-averaging the quasi-energy we can make the second term disappear, where we define the time-average as

$$\{Q\}_T = \frac{1}{T}\int_{-T/2}^{T/2} Q(t)dt. \tag{4.8}$$

We can then similarly relate properties (time-dependent) to the quasi-energy derivative

$$\frac{d\{Q\}_T}{d\epsilon_x(\omega_k)} = \Big\{\langle\tilde{0}|\frac{\partial\hat{H}}{\partial\epsilon_x(\omega_k)}|\tilde{0}\rangle\Big\}_T . \tag{4.9}$$

An expression of the linear response functions can then straightforwardly be attained by differentiating the time-averaged quasi-energy with respect to the field strength twice, and expanding the expectation value of the perturbation operator $\hat{X}$ as in equation 4.5

$$\frac{d^2\{Q\}_T}{d\epsilon_A(\omega_a)d\epsilon_B(\omega_b)}\bigg|_{\epsilon=0} = \frac{1}{2}\Big(\langle\langle\hat{A};\hat{B}\rangle\rangle_{\omega_a} + \langle\langle\hat{B};\hat{A}\rangle\rangle_{\omega_b}\Big)\delta(\omega_a+\omega_b). \tag{4.10}$$

Here, the delta function ensures that the response function is zero unless $\omega_b = -\omega_a$.

The linear response functions may be expressed as a sum over states formula for exact states as

$$\langle\langle\hat{X};\hat{Y}\rangle\rangle_{\omega_b} = \frac{1}{\hbar}\sum_n\Big(\frac{\langle 0|\hat{X}|n\rangle\langle n|\hat{Y}|0\rangle}{\omega_n-\omega_b} + \frac{\langle 0|\hat{Y}|n\rangle\langle n|\hat{X}|0\rangle}{\omega_n+\omega_b}\Big). \tag{4.11}$$

However, typically this expression is not used for practical applications. Therefore, we will in the next section proceed to derive approximate expressions by which we can evaluate the linear response functions.

4.2 Linear response for approximate wavefunctions

In the previous subsection, we did not assume any particular wave function ansatz. Therefore, in this section, we now derive explicitly an approximate wave function at the HF level of theory. It should be noted that the papers take departure in Kohn-Sham DFT, which also builds on a Slater determinant and thus to a large degree is similar to the HF theory presented here. The main exception is the additional terms arising from the exchange-correlation functional (cf, Paper II). The HF wave function is parametrized as

$$|\tilde{0}\rangle = e^{-\hat{\kappa}(t)}|0\rangle \tag{4.12}$$

where $|0\rangle$ is a Slater-determinant and $\hat{\kappa}(t)$ is the time-dependent orbital-rotation operator, to be defined below. By inserting the Hamiltonian, $\hat{H}$, defined in equations 4.2 and 4.3 into 4.8, and using the HF wave function defined as in equation 4.12 we obtain

$$\{Q\}_T = \Big\{\langle\tilde{0}|\Big(\hat{H}_0 - i\frac{\partial}{\partial t}\Big)|\tilde{0}\rangle\Big\}_T + \sum_k\sum_X \epsilon_X(\omega_k)\Big\{\langle\tilde{0}|\hat{X}|\tilde{0}\rangle\Big\}_T, \tag{4.13}$$

where the part with the external field has been rearranged to be last. A perturbation expansion of the quasi-energy can now be obtained from the perturbation expansion of the orbital-rotation-operator. Here expansion to first order is sufficient, and we define the first order (Fourier transformed) orbital-transformation operator as

$$\hat{\kappa}(t) = \sum_k \sum_\mu \Big(\kappa_\mu(\omega_k) q_\mu^\dagger - \kappa_\mu^*(-\omega_k) q_\mu \Big) e^{-i\omega_k t}, \tag{4.14}$$

where the excitation operators $q_{ai}^\dagger = \hat{a}_a^\dagger \hat{a}_i$ are products of creation and annihilation operators, and $\kappa_{ai}(\omega_k) = \epsilon_X(\omega_k)\kappa_{ai}^{\omega_k}$ are variational parameters linear in the field strength. Note spinor indices for occupied (i) and virtual spinors (a) are collected into one index (μ).

Using the Baker-Campbell-Hausdorff (BCH) expansion in equation 4.13 and then inserting the orbital-rotation operator we thereby obtain the following expression for the time-averaged quasi-energy for second order perturbations

$$\begin{aligned}\{Q_T^{(2)}\} =& \frac{1}{2} \sum_{k,l} \Big(\bar{\boldsymbol{\kappa}}^\dagger(-\omega_k) \Big(\boldsymbol{E}_0^{[2]} - \omega_k \boldsymbol{S}^{[2]} \Big) \bar{\boldsymbol{\kappa}}(\omega_l) \Big) \delta(\omega_k + \omega_l) \\ &+ \sum_{k,l} \sum_X \epsilon_X(\omega_k) \bar{\boldsymbol{\kappa}}^\dagger(-\omega_l) \boldsymbol{E}_Y \delta(\omega_k + \omega_l). \end{aligned} \tag{4.15}$$

We have introduced a vector notation $\bar{\boldsymbol{\kappa}}(\omega_k) = (\boldsymbol{\kappa}(\omega_k), \boldsymbol{\kappa}^*(-\omega_k))^T$ for the orbital-rotation operators and $\boldsymbol{E}_Y^{[1]} = (\boldsymbol{g}_Y, \boldsymbol{g}_Y^*)^T$ for the property gradient with elements

$$g_\mu^Y = \langle 0 | [-\hat{q}_\mu, \hat{Y}] | 0 \rangle. \tag{4.16}$$

Finally, we have in equation 4.15 introduced the electronic Hessian, $\boldsymbol{E}_0^{[2]}$, and metric, $\boldsymbol{S}^{[2]}$, matrices

$$\boldsymbol{E}_0^{[2]} = \begin{pmatrix} \boldsymbol{A} & \boldsymbol{B} \\ \boldsymbol{B}^* & \boldsymbol{A}^* \end{pmatrix} \qquad \boldsymbol{S}^{[2]} = \begin{pmatrix} \boldsymbol{\Sigma} & \boldsymbol{\Delta} \\ -\boldsymbol{\Delta}^* & -\boldsymbol{\Sigma}^* \end{pmatrix}, \tag{4.17}$$

with the elements

$$A_{\mu\gamma} = \langle 0 | [-q_\mu, [q_\gamma^\dagger, H_0]] | 0 \rangle \qquad B_{\mu\gamma} = \langle 0 | [q_\mu, [q_\gamma, H_0]] | 0 \rangle \tag{4.18}$$

$$\Sigma_{\mu,\gamma} = \langle 0 | [-q_\mu, q_\gamma^\dagger] | 0 \rangle \qquad \Delta_{\mu,\gamma} = \langle 0 | [q_\mu, q_\gamma] | 0 \rangle. \tag{4.19}$$

From this, it is then possible to define an expression for the linear response functions as in equation 4.10

$$\langle\langle X; Y \rangle\rangle_{\omega_k} = -\boldsymbol{E}_X^{[1]\dagger} (\boldsymbol{E}_0^{[2]} - \omega_k \boldsymbol{S}^{[2]})^{-1} \boldsymbol{E}_Y^{[1]}. \tag{4.20}$$

In practice, explicit construction of the electronic Hessian is unfeasible for all but the smallest systems. Therefore, response functions are found by solving the linear response equations in a reduced space

$$(\boldsymbol{E}_0^{[2]} - \omega_k \boldsymbol{S}^{[2]})\boldsymbol{X}_Y(\omega_k) = -\boldsymbol{E}_Y^{[1]}, \tag{4.21}$$

where the solution vector $X_B(\omega)$ is expanded in a set of trial vectors[42]

$$\boldsymbol{X}_B(\omega_k) = \sum_{i=1}^{n} b_i a_{Y;i}(\omega_k); \quad B = [b_1\ b_2\ \ldots b_n]. \tag{4.22}$$

This leads to the n-dimensional reduced linear response equation, where all calculations previously involving the Hessian now instead use sigma vectors

$$\boldsymbol{\sigma}_i = \boldsymbol{E}_0^{[2]}\mathbf{b}_i, \tag{4.23}$$

which avoids the construction and storage of the full Hessian.

4.3 Damped linear response theory

Examining the response function for an exact wave function in equation 4.11 shows that there will be singularities for the linear response functions in resonant regions. Although this is indeed exploited in the calculation of excitation energies, it is unphysical. To remedy this issue, we first examine the excited state wave functions: Letting the state $|n\rangle$ be an excited state solution to the time-independent Schrödinger equation with eigenvalue E_n means that[39,43]

$$|n(t)\rangle = e^{-iE_n t}|n\rangle, \tag{4.24}$$

will satisfy equation 4.1. However, the norm of $|n(t)\rangle$ is constant in time, i.e., the system has an infinite lifetime, while excited states generally decay through various mechanisms. The infinite lifetime can be avoided by introducing a (phenomenological) damping, $i\gamma$,[44,45,46,47]

$$|\bar{n}(t)\rangle = e^{-i(E_n - i\gamma)t}|n\rangle, \tag{4.25}$$

leading to complex excited state energies ($E_n \rightarrow E_n - i\gamma$). The $|\bar{n}(t)\rangle$ state is denoted a damped excited state, and using this state in the response equations corresponds to replacing the excitation energy ω_i with $\omega_i + i\gamma$. With this, equation 4.21 becomes[44,45]

$$(\boldsymbol{E}_0^{[2]} - (\omega_k + i\gamma)\boldsymbol{S}^{[2]})\boldsymbol{X}_Y(\omega_k) = -\boldsymbol{E}_Y^{[1]}. \tag{4.26}$$

The dampening factor (here taken to common for all excited states) accounts for the finite lifetime of the excited states and thus γ can be regarded as being the effective inverse lifetime[39,45]. In Paper II, it is shown how damped response theory can be formulated in a relativistic PE framework.

4.4 Linear response properties

In this section, we will outline some of the molecular properties that can be obtained by using linear response theory. We will describe the physics underlying the properties and then relate them to different spectroscopic techniques. Moreover, we will employ exact state linear response theory to highlight the physical quantities.

4.4.1 UV-Vis absorption

Electronic transitions induced by electromagnetic (EM) radiation in the range of 200-800 nm can be probed through UV-Vis absorption spectroscopy. In this part of the EM spectrum, the wavelengths are typically so long compared to the molecular species of interest that the EM field can be regarded as uniform. Therefore, we can motivate the use of the electric-dipole approximation. The EM field can thereby be regarded as perturbing the electron density by exciting an electron from the ground state and creating an induced dipole moment μ. The strength of this dipole moment can be calculated as an expectation value between that of the ground state and an excited electronic state as $\langle 0|\mu_z|n\rangle$, where we have assumed the external field to be applied along the z-axis. This is more commonly known as the electric dipole transition moment. The measure of the ability to acquire an electric dipole moment of a molecule is the polarizability α. This can be related to the transition moments through perturbation theory, resulting in a sum over-states formula analogous to Eq. 4.11

$$\alpha_{\alpha\beta}(\omega_b) = \langle\langle \hat{\mu}_\alpha; \hat{\mu}_\beta \rangle\rangle_{\omega_b} = \frac{1}{\hbar} \sum_n \Big(\frac{\langle 0|\hat{\mu}_\alpha|n\rangle\langle n|\hat{\mu}_\beta|0\rangle}{\omega_n - \omega_b} + \frac{\langle 0|\hat{\mu}_\beta|n\rangle\langle n|\hat{\mu}_\alpha|0\rangle}{\omega_n + \omega_b} \Big). \tag{4.27}$$

This is a concrete example of a linear response function. From the poles of $\boldsymbol{\alpha}$, i.e., where the frequency, ω_b, of the perturbing field approaches ω_n ($\omega_n \rightarrow \omega_b$), we can identify excitation energies in a spectrum. The residues then contain transition dipole moments which can be directly related to the oscillator strengths of transitions. To better compare results from calculations with that of experiments, one typically applies some type of broadening function to the individual oscillator strengths. In reality, this broadening corresponds to a variety of effects, such as that of the finite lifetime of the excited states and vibronic transitions. Finally, we note that certain electronic transitions may be forbidden due to spatial or spin symmetry. However, the spin symmetry requirements can be lifted when assuming a four or two-component wave function, since spin is then no longer a well-defined quantum number.

4.4.2 Electronic circular dichroism

In the previous sections, we assumed that the EM field was plane-polarized. However, this is not always the case. When the electric (and magnetic) component rotates around the axis of propagation, we have what is called circularly polarized light (CPL). Moreover, depending on whether the rotation is clockwise or anticlockwise, we have *right* and *left* CPL. Spectroscopies that employ CPL are generally used for molecules with non-superimposable mirror images, defined as *chiral*. The two mirror-images of a chiral molecule are called *enantiomers*, and will interact differently with CPL depending on whether it is L or R-CPL. The differential absorption between L and R-CPL can thus be used to establish what enantiomers that are prevalent in a sample. This type of spectroscopy, called *Electronic circular dichroism* (ECD), is highly useful since the physical properties of two enantiomers are virtually identical, but the way they interact with other molecules can be very different.

The electronic transitions in ECD can in a similar fashion to UV-Vis be related to the fact that the EM field creates induced dipole moments. However, in contrast to UV-Vis, there is also a contribution from the magnetic component of the field. The equation that relates these quantities was established by Rosenfeld 75 years ago through perturbation theory[48]

$$\langle \hat{\boldsymbol{\mu}} \rangle = \boldsymbol{\alpha} \boldsymbol{E} + \frac{1}{\omega} \boldsymbol{\beta} \frac{\partial \boldsymbol{B}}{\partial t}. \tag{4.28}$$

Where the first term is the contribution due to the electric dipole-dipole polarizability tensor $\boldsymbol{\alpha}$ and the electric field $\boldsymbol{E}$, whereas the second is the $\boldsymbol{\beta}$ tensor times an alternating magnetic field $\boldsymbol{B}$. For chiroptical properties such as ECD, the $\boldsymbol{\beta}$ tensor is the most essential quantity and can be expressed as a sum over states formula

$$\beta_{\alpha\beta}(\omega) = \langle\langle \hat{\mu}_\alpha ; \hat{m}_\beta \rangle\rangle_\omega = -\frac{2\omega}{\hbar} \sum_{n \neq 0} \frac{\mathrm{Im}(\langle 0|\hat{\mu}_\alpha|n\rangle\langle n|\hat{m}_\beta|0\rangle)}{\omega_{n0}^2 - \omega^2}. \tag{4.29}$$

For ECD, the excitation energies of electronic transitions correspond to poles in the expression (zeros in the denominator), and the associated residues can be used to calculate the intensities. The residues are called rotatory strengths R_{n0} and can be calculated as the dot product between the electric and magnetic transition dipole moments

$$R_{n0} = \mathrm{Im}(\langle 0|\hat{\boldsymbol{\mu}}|n\rangle \cdot \langle n|\hat{\boldsymbol{m}}|0\rangle). \tag{4.30}$$

As seen from Eq. 4.29, this corresponds to the residues of the response function. The rotatory strengths are similar to oscillator strengths. However, they can be both negative and positive, since they are related to differential absorption. Similarly to UV-Vis, some type of broadening is also usually applied to the individual rotatory strengths to yield a better comparison with experiment.

Chapter 5

Research and Outlook

5.1 Summaries of papers

Paper I: Investigating the influence of relativistic effects on absorption spectra for platinum complexes with light-activated activity against cancer cells

Traditional square-planar Platinum(II) complexes used in chemotherapy lead to severe side effects due to side reactions with other bio-molecules than DNA in cancer cells. Therefore, new types of octahedral Platinum(IV) complexes that can be ingested in an inactive form and then transformed into the active form at the site of a tumour utilizing light have been studied. Earlier theoretical studies with non-relativistic response theory have investigated the activation mechanism, mainly by analyzing calculated UV-vis spectra. In this paper, we report the first investigation of the impact of relativistic effects on the UV-vis spectra of these octahedral Platinum complexes. For that purpose, the absorption spectra of two Platinum complexes were investigated. Hence, Time dependent-density functional theory (TD-DFT) calculations were carried out with the functional B3LYP and its range-separated version CAM-B3LYP with non-relativistic (NR), scalar relativistic (SR), and 4c Hamiltonians in the DIRAC program. Additionally, calculations including an effective core potential were done with the DALTON program. Not surprisingly, the spectra from the NR Hamiltonian were altered significantly when compared to a 4c or SR Hamiltonian. Furthermore, the results show that a SR Hamiltonian is enough to reproduce the most dominant transitions in the 4c spectra. However, a more careful analysis in regions outside the most intense ones, shows that many transitions are spin-mixed and have no counterpart in SR (and NR) calculations since the latter does not include spin-orbit coupling. Many of these transitions were also in the lower end of the spectra (above 300 nm)

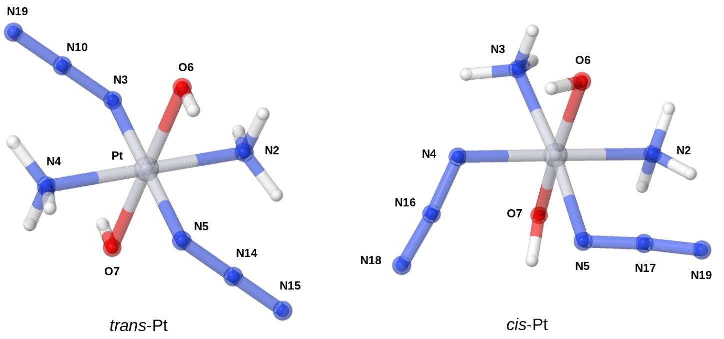

trans-Pt

cis-Pt

Figure 5.1: Optimized structures of the two studied complexes. (Reproduced from Ref. 6 with permission from the Royal Society of Chemistry)

where experiments have shown that light activation can occur. Thus, including spin-orbit coupling might be crucial to correctly understand what electronically excited states that are active when the complexes are active against cancer cells. The results from an effective-core potential yielded the same results as that of employing a SR Hamiltonian. Finally, to note is that we obtained the same conclusions regardless of whether using B3LYP or CAM-B3LYP.

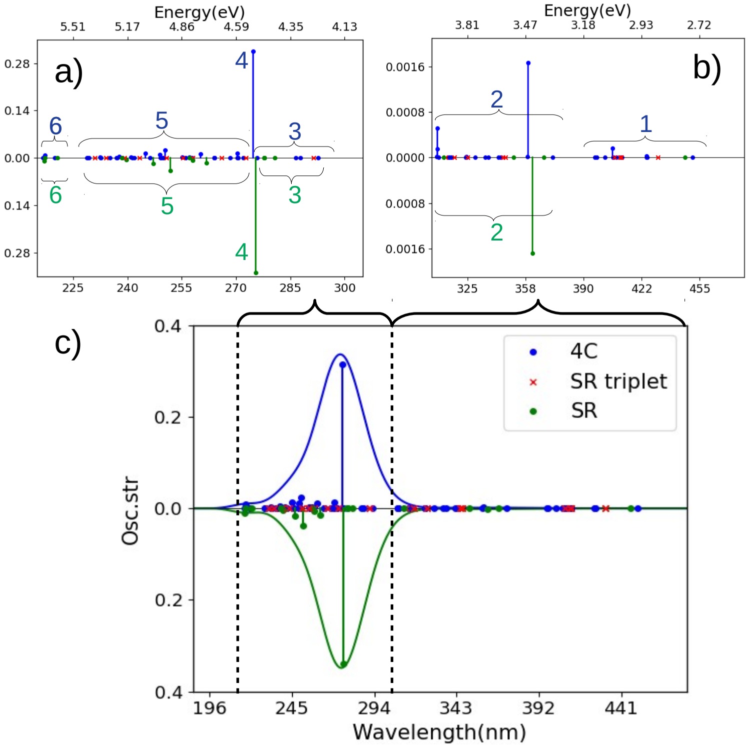

Figure 5.2: Spectra for *trans*-Pt calculated with CAM-B3LYP and SR or 4c Hamiltonians. (a) and (b) are magnified for 215–305 nm and 305–480 nm. (c) shows the full spectrum. The SR calculation is always shown along a mirrored y-axis for clarity. (Reproduced from Ref. 6 with permission from the Royal Society of Chemistry)

Paper II: Polarizable embedding complex polarization propagator in a four and two-component frameworks

In paper II, we develop the theory and implementation of damped response theory in a relativistic framework with the inclusion of environmental effects through the polarizable embedding model. This implementation has been done in the Dirac program.

The response equations in equation 4.26 will not fundamentally change in a relativistic framework and can be modified to include a polarizable environment, here represented by site multipoles and site-polarizabilities. The derivation proceeds similarly to the vacuum case, but with the vacuum Hamiltonian augmented with the operators defined in equation 3.7 and 3.17

$$\hat{H}_{tot} = \hat{H} + \Big(\hat{V}^{es} - \frac{1}{2}\langle\tilde{0}|\hat{\boldsymbol{\mathcal{E}}}|\tilde{0}\rangle\mathbf{R}\hat{\boldsymbol{\mathcal{E}}}\Big), \tag{5.1}$$

leading to the following modification of the time-averaged quasi-energy (cf. equation 4.13)

$$\{Q\}_T = \left\{\langle\tilde{0}|\left(\left[\hat{H} - i\frac{\partial}{\partial t}\right] + \hat{V}^{es} - \frac{1}{2}\langle\tilde{0}|\hat{\boldsymbol{\mathcal{E}}}|\tilde{0}\rangle\mathbf{R}\hat{\boldsymbol{\mathcal{E}}}\right)|\tilde{0}\rangle\right\}_T . \tag{5.2}$$

Before moving on, we note that there will also be a contribution due to the perturbing fields' interaction with the environment. While this contribution is considered in Paper II, it is for brevity left out of this overview. The derivation for the response equations follows the vacuum case in equations 4.13–4.20, and the introduction of a finite lifetime is done as illustrated in equation 4.26. Thus, it can be developed using a BCH expansion, as in equations 4.13–4.19, leading to equation 4.26, but with a $\mathbf{E}^{[2]}$ matrix modified to include the polarizable embedding contributions. The modified $\mathbf{E}^{[2]}$ matrix has elements

$$A_{\mu,\gamma} = -\langle 0|[q_\mu, [q_\gamma^\dagger, \hat{f} + \hat{V}^g]]|0\rangle + \langle 0|[q_\mu, \hat{\boldsymbol{\mathcal{E}}}^e]|0\rangle^T\mathbf{R}\langle 0|[q_\gamma^\dagger, \hat{\boldsymbol{\mathcal{E}}}^e]|0\rangle \tag{5.3}$$

$$B_{\mu,\gamma} = \langle 0|[q_\mu, [q_\gamma, \hat{f} + \hat{V}^g]]|0\rangle - \langle 0|[q_\mu, \hat{\boldsymbol{\mathcal{E}}}^e]|0\rangle^T\mathbf{R}\langle 0|[q_\gamma, \hat{\boldsymbol{\mathcal{E}}}^e]|0\rangle, \tag{5.4}$$

where the Fock operator, $\hat{f}$, and environment operator were defined in Chapters 2 and 3, respectively. To note is that the Hessian elements in the paper look slightly different since we are here formulating the theory with respect HF while the paper is focused on KS-DFT. However, the derivations and the corresponding terms are analogous, with the only change being one additional term with respect to the Hartree-exchange-correlation kernel.

The reduced equations where we have introduced a trial vector $\mathbf{X}_B$ (see equation 4.21) will naturally also be modified by the PE operator. The modification will manifest in two additional terms to the sigma vectors

$$\sigma_\mu = \langle 0|[-q_\mu, \tilde{f} + \tilde{V}^g]|0\rangle + \langle 0|\tilde{\boldsymbol{\mathcal{E}}}^e|0\rangle\mathbf{R}^T\langle 0|[-q_\mu, \hat{\boldsymbol{\mathcal{E}}}^e]|0\rangle, \tag{5.5}$$

where we have defined the so-called one-index transformed operators 4.26. The additional terms due to the PE environment are the term including $\tilde{V}^g$ and the last term.

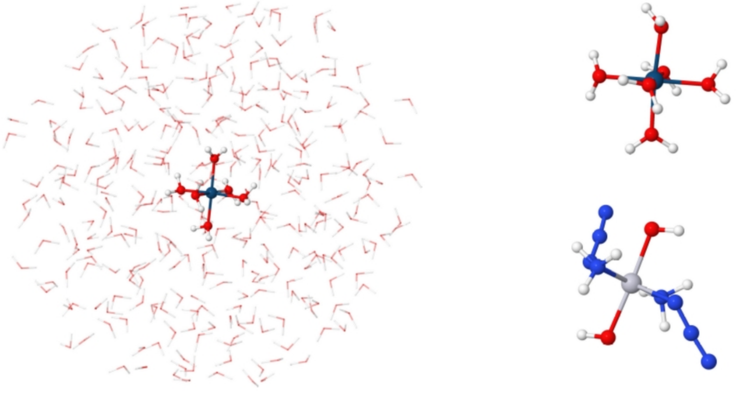

Figure 5.3: The solvated systems used in the PE calculations for $[Rh(H_2O)_6]^{3+}$ and $[Ir(H_2O)_6]^{3+}$ (shown with and without solvent, using $[Ir(H_2O)_6]^{3+}$ as example). The solvated *trans-trans-trans*-$Pt(N_3)_2(OH)_2(NH_3)$ (also shown without solvent below $[Ir(H_2O)_6]^{3+}$) is treated similarly. (Reproduced from Ref. 49 with permission from the American Chemical Society)

To ensure that the method works, we tested it on the two metal complexes $[Rh(H_2O)_6]^{3+}$ and $[Ir(H_2O)_6]^{3+}$ immersed in aqueous solution. We calculate UV-Vis and X-ray absorption (XAS) spectra, using both X2C and 4c. From the results, we estimate the solvent effects on the spectra. We divide the solvent effect into two contributions; electronic effects (from PE) and the structural perturbation (from optimization in solvent). We conclude that the structural effects are the largest, but that both contributions are essential to obtain accurate properties. We also take into account the use of an effective external field (EEF), and find that it does not alter the excitation energies, but that it has a considerable impact on the absorption cross-section. Moreover, we compare the results of using a 4c Hamiltonian to that of X2C and show that X2C is sufficient to reproduce 4c results for all solvent shifts. Finally, we compare the effect of using electrostatic embedding to that of polarizable embedding by calculating UV-Vis spectra of *trans-trans-trans*-$[Pt(N_3)_2(OH)_2(NH_3)_2]$. Our results show that most of the electronic solvent effects are captured by including the electrostatic multipoles in the environment and that the excitation energies change little by including polarization. However, the polarization has a significant effect on the absorption cross-section.

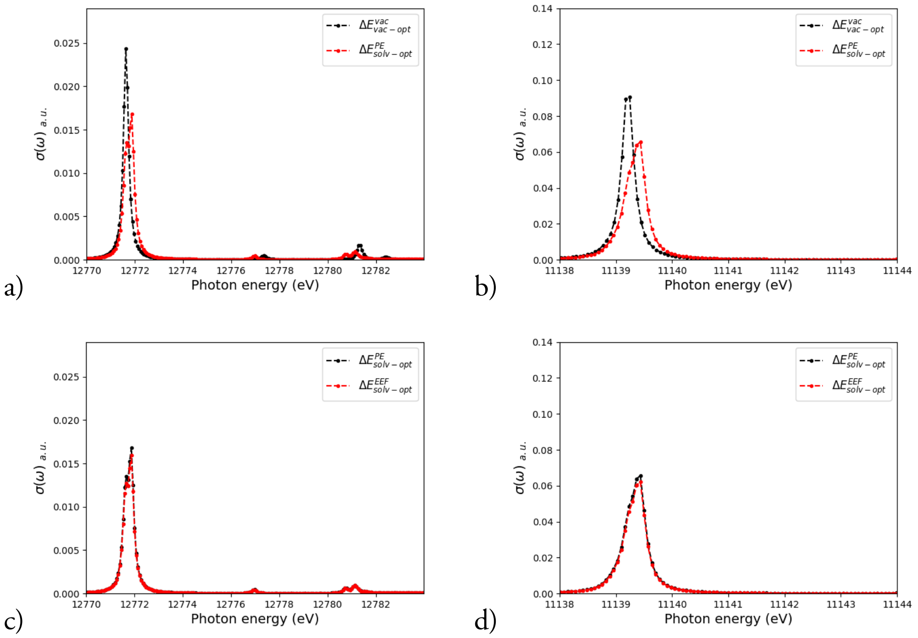

Figure 5.4: L-edge spectra of $[Ir(H_2O)_6]^{3+}$. The panels (a) and (b) compares of vacuum and PE calculations for (a) L_{II}-edge and (b) the L_{III}-edge, while panels (c) and (d) compares PE calculations environment with and without EEF effects for (c) L_{II}-edge and (d) the L_{III}-edge. (Reproduced from Ref. 49 with permission from the American Chemical Society)

Paper III: New relativistic quantum chemical methods for understanding light-induced therapeutics

This paper is a short overview/perspective on the field of investigating light-activated chemotherapy with theoretical methods. As examples, we discuss the method introduced in Paper II as well as other complexes with a light-induced reaction mechanism that have been investigated with theoretical methods. We also discuss methods based on TD-DFT.

Understanding the underlying photo-physical properties of potential pro-drug candidates is critical, and for this, theoretical methods have been shown to provide an indispensable tool. However, there are certain factors one should take into consideration when choosing a model. In this perspective we explore three of these factors: i) relativistic effects, ii) multi-configurational effects and iii) explicit solvent effects.

(i) Since the target complexes typically include heavy metals such as platinum or gold, it is important to consider relativistic effects. We divide relativistic effects into scalar relativistic effects (SR) and spin-orbit coupling (SO). While there are various ways to include scalar relativistic and SO effects, the most rigorous way to obtain both effects is to solve the Dirac equation. From the Dirac equation, we obtain a four-component wave function which in turn can be divided into a large component and small component. Each component also has α and β spin components leading to the total four-component wave function. Notably, the α and β components are allowed to mix, unlike in non-relativistic theory. The consequence of this is that previously spin-forbidden transitions can occur. It is also possible to formulate variations of the theory where the solutions to the large and small components can be decoupled, resulting in a two-component wavefunction. These types of methods are considerably cheaper compared to four component methods, yet still retain treatment of both scalar relativistic effects and spin-orbit coupling.

(ii) Relativistic TD-DFT has been quite successful in predicting UV-Vis absorption spectra of platinum complexes employed in photo-activated chemotherapy (PACT). Yet, TD-DFT assumes vertical transitions around the ground-state structure and may become inadequate for investigating ligand dissociation, where static correlation becomes important. A more accurate description of this process can be obtained by multi-configurational methods. One of these methods, CASSCF, has been used in previous studies together with its PT2 corrected variant CASPT2. Although accurate, these methods are limited by the size of the active space. A new variant known as density matrix renormalization group (DMRG) theory, enables the inclusion of larger active spaces and has also recently been applied to describe dissociation curves of *trans-trans-trans*-$[Pt(N_3)_2(OH)_2(NH_3)_2]$.

(iii) The photo-activation of the complexes always takes place in an aqueous medium with solvated bio-molecules. Thus, to mimic experimental conditions, the inclusion of a solvent must be included in our models. Typically, this has been done by modelling the solvent as a dielectric medium in continuum models. However, continuum models are particularly problematic for solvents with the ability to form hydrogen bonds. These could of course be modelled by extending the size of the system, to retain the explicit treatment of the environment, but this would drastically increase the computational cost. A better way is to divide the system into a region treated by methods from quantum chemistry (QM) and then treat the environment by classical molecular mechanics methods (MM). This enables an explicit treatment of the environment. Yet, standard QM/MM models do not allow for the mutual polarization of the QM and environment regions, which is necessary to accurately model processes involving excited states. A model that takes this into account is the polarizable embedding (PE) model. In the perspective, we discuss the method in paper II that combines the PE model with a relativistic treatment of the wave function in a linear response framework. We also discuss how this method has been successfully applied on the *trans-trans-trans*-$[Pt(N_3)_2(OH)_2(NH_3)_2]$ complex.

Paper IV: A method to capture the large relativistic and solvent effects on UV-vis spectra of photo-activated metal complexes

In Paper IV, we embark on a mission to more rigorously explore the photo-physical properties of the *trans-trans-trans*-$[\mathrm{Pt}(\mathrm{N}_3)_2(\mathrm{OH})_2(\mathrm{NH}_3)_2]$ complex in aqueous environments. We first investigate a single structure obtained by optimizing *trans-trans-trans*-$[\mathrm{Pt}(\mathrm{N}_3)_2(\mathrm{OH})_2(\mathrm{NH}_3)_2]$ complex in water. We take the structure investigated in paper II, which was first optimized at the QM/MM level in a 35 X 35 X 35 box of water molecules (with water frozen). We make a cutout of the complex and the surrounding water molecules within 6 Å of the complex. We then optimize this cluster, where we allow the water molecules within 4 Å to relax while the rest are kept frozen. This optimization was first done with the semiempirical PBEh-3c method and then subsequently optimized using the BP86 functional. We then re-insert this optimized cluster into the original water box and make a new cutout including all water molecules within 10 Å of the complex. From this procedure, we obtain four different structures, the 10 and 6Å clusters optimized at both the PBEh-3c and BP86 levels. We use the PE-X2C-CPP method developed in paper II to compute the UV-Vis absorption spectra of these structures. From the results, we see that changing the structure from PBEh-3c to BP86 is accompanied by a large shift in the spectra.

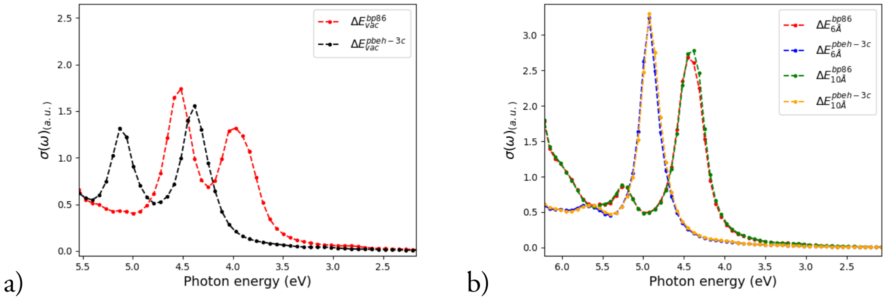

Figure 5.5: (a) UV-vis absorption spectra calculated in vacuum with structures obtained from PBEh-3c and BP86 (in solvent). (b) UV-vis absorption spectra were calculated with the structures from (a) including PE for 6 and 10 Å. All spectra are calculated with X2C-CAM-B3LYP.

However, changing the environment from the 6 to the 10 Å cluster only has a minor impact on the spectra. We also make the comparison using a spin-free Hamiltonian and can draw the same conclusions. Moreover, to ensure that the complex is sufficient as the QM part of the system, we compare with calculations where we have included the five closest water molecules in the QM region. The effects on the spectra are small, and we can thus safely assume that it is enough to include the complex in the QM region.

Next, we turn to investigate the UV-Vis absorption spectra for multiple structures. We construct a force field for the *trans-trans-trans*-[Pt$(N_3)_2(OH)_2(NH_3)_2$] complex and carry out classical molecular dynamics simulations. From the trajectory, we extract 49 clusters including the complex and the nearest water molecules within 6 Å. We then carry out subsequent optimizations on these clusters using the same procedure as described for the static structure. We carry out calculations using PE-X2C-CPP with the CAM-B3LYP functional to obtain UV-Vis spectra for the 49 clusters. We calculate the average of the maximum peak for the spectra of the clusters and compare it with that of experiment. The average peak maximum is at 4.79 eV, which is somewhat blue-shifted compared to experiment (4.35 eV). We argue that this might be caused by the choice of functional which has been known to lead to blue-shifted spectra compared to other transition metal complexes. Alternatively, the error could be caused by the procedure in which the structures were obtained. Nevertheless, we can still see that there is a huge impact of the solvent on the resulting spectra, which emphasizes the further need to explicitly include the solvent molecules in calculations.

Paper V: Electronic Circular Dichroism at the level of four-component Kohn–Sham density functional theory

Molecules with mirror images that can not be superimposed on one another are said to be chiral. The two mirror images of a chiral species (called enantiomers) have similar physical properties (e.g. identical UV-Vis spectra), but can have different reaction mechanisms depending on the enantiomer. This has serious implications in for instance pharmacy, where a chiral drug can lead to a cure for one enantiomer, while the other enantiomer might have unforeseen side effects. Thus, being able to identify which enantiomers are prevalent in a sample is crucial. A method to distinguish between the different enantiomers can be done by exploiting the fact that they interact differently with *left* (L) and *right* (R) circularly polarized light (CPL). The properties associated with this are called optical rotatory dispersion (ORD) and electronic circular dichroism (ECD).

Theoretical methods provide an important role in assisting the interpretation of ORD and ECD spectra and can be especially useful in assigning absolute configurations. In this paper, we devise a method to calculate both ORD and ECD in a four-component Kohn-Sham framework. In a linear response framework both properties can be related to the electric dipole - magnetic dipole polarizability tensor $\langle\langle \hat{\mu}_X; \hat{m}_Y \rangle\rangle_{\omega_k}$ which is the response function for the magnetic component of the electromagnetic field. However, in contrast to regular linear response theory, we take into account the finite lifetime of the excited states by introducing the phenomenological damping parameter γ_n into the response functions. This causes the equations and their solutions to become complex, with the imaginary and real parts of the solutions being associated with ORD and ECD respectively. From the imaginary part of $\langle\langle\hat{\mu}_X;\hat{m}_Y\rangle\rangle_{\omega_k}$ we obtain the ORD as

$$\Delta\theta = -\frac{1}{3}\omega\mu_0 l N \sum_{X\in\{x,y,z\}} \mathrm{Im}\langle\langle\hat{\mu}_X;\hat{m}_X\rangle\rangle_\omega, \tag{5.6}$$

where μ_0 is the permeability of vacuum, l is the path length and N (m^{-3}) is the number density of molecules. The real part of the response function can then be used to calculate circular dichroism as

$$\Delta\epsilon(\omega) = -6.533\omega \sum_{X\in\{x,y,z\}} \mathrm{Re}\langle\langle\hat{\mu}_X;\hat{m}_X\rangle\rangle_\omega. \tag{5.7}$$

We formulate the theory in a relativistic four-component framework. The corresponding changes are mainly seen in the operator for the magnetic dipole moment which takes the following form

$$\hat{\mathbf{m}}(\mathbf{R}) = -\frac{1}{2}\Big((\hat{\mathbf{r}}-\mathbf{R})\times\hat{\mathbf{j}}\Big), \tag{5.8}$$

where $\hat{\mathbf{r}}$ is the position operator, $\hat{\mathbf{j}}$ is the current density operator and $\mathbf{R}$ is the origin. To test the method we carry out ORD and ECD calculations for the series 3R-halide-1-butyn of organic molecules, with the halide being equal to fluorine, chlorine, bromine and iodine. The ORD calculations are carried out for one frequency. They show that relativistic effects become more important for heavier molecular species as expected. Moreover, the convergence with respect to the basis set is investigated and also the influence of the choice of functional. Finally, we calculate ECD spectra using the aug-cc-pVTZ basis set (except for iodine where the Dyall(cv3z) triple-zeta basis set was employed) and the B3LYP functional. All calculations were carried out both in a 4c relativistic framework and a one-component non-relativistic framework. For the compounds containing fluorine and chlorine the one - and four-component results are in correspondence, while small changes start to occur for bromine and larger discrepancies are seen for certain parts of the spectra of the iodine compound.

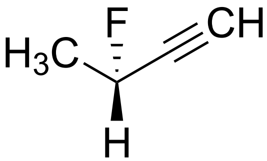

Figure 5.6: Chemical structure of 3*R*-fluoro-1-butyne.

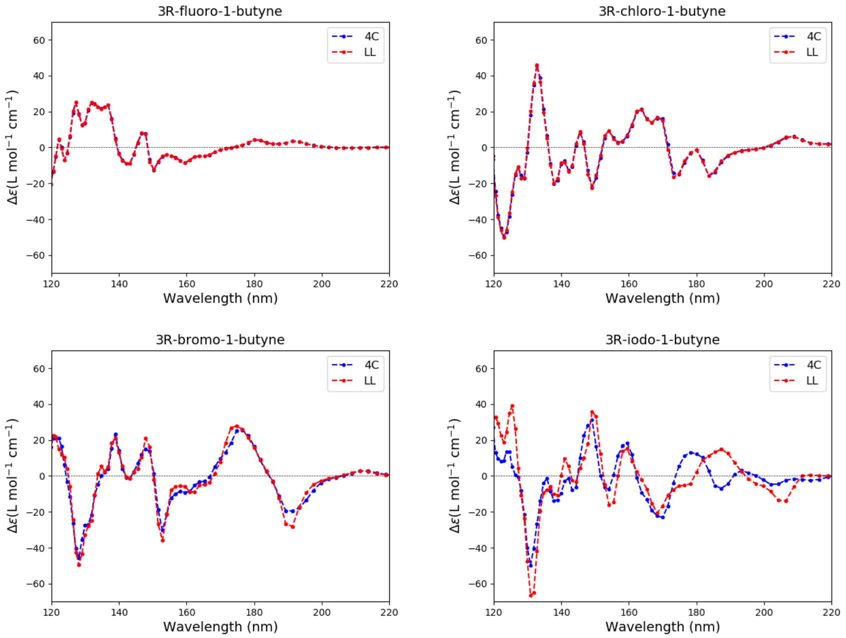

Figure 5.7: Comparison of relativistic (blue) and nonrelativistic (red) ECD spectra of $3R$-fluoro-1-butyne, $3R$-chloro-1-butyne, $3R$-bromo-1-butyne and $3R$-iodo-1-butyne. All calculations were carried out in the gas phase using the B3LYP functional in combination with the aug-cc-pVTZ basis set and geometries optimized at the B3LYP/aug-cc-pVDZ level of theory.

Paper VI: A method to explore the combined impact of relativistic and solvent effects on electronic circular dichroism spectra

Previous studies (such as paper V) have extended relativistic linear response theory to be able to calculate ECD and ORD spectra. It has been shown that relativistic effects on chiroptical properties can be significant for molecules that are comprised of heavy elements, and also in the X-ray regime. Similar studies have been carried out for solvent effects. They have shown that both the electronic and dynamic effects of a solvent yield substantial effects on chiroptical properties. Yet, no studies exist where both effects are accounted for. We, therefore, devise such a method in this study. In contrast to paper V, we calculate residues of the response function

$$ {}^{n}R_{xy} = \lim_{\omega_{n0}\to\omega} (\omega_{n0}-\omega)\,\mathrm{Im}\langle\langle\hat{\mu}_x;\hat{m}_y\rangle\rangle_{\omega}, \tag{5.9} $$

where ${}^{n}R_{xy}$ are the so-called rotatory strengths. By solving the linear response eigenvalue equation we calculate excitation energies and transition moments (electric and magnetic) from which we can calculate the rotatory strengths (defined as in Eq. 4.30). We work in a four- or two-component relativistic framework, which entails a modification of the expression for the magnetic and electric dipole moments as defined in the summary of paper V. The polarizable embedding model is used to describe how the environment (defined as fragments represented by static localized multipole moments and site polarizabilities) interacts with the electron density in the QM region. Changes concerning the linear response framework are principally seen in the electronic Hessian, as described in the summary of paper II. To illustrate our method we employ the two stereoisomers (S and R) of the organic molecule 2-Bromo-2-iodoacetic acid and its conjugate base 2-Bromo-2-iodoacetate as test systems. We first investigate the relativistic effects by calculating the ECD spectra with various Hamiltonians ranging from the four-component Dirac Coulomb Hamiltonian to the non-relativistic Lévy-Leblond Hamiltonian.

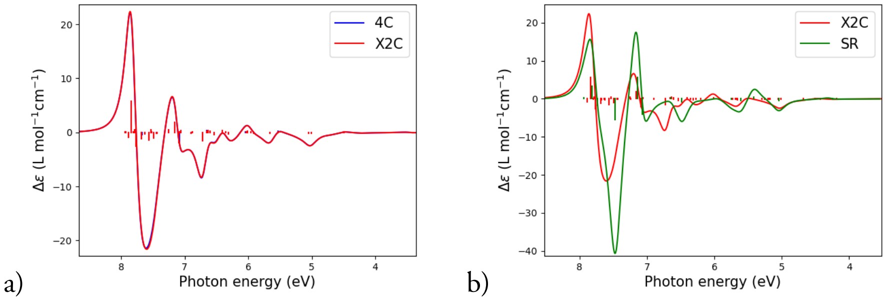

Figure 5.8: ECD spectra for (S)-2-bromo-2-iodoacetic acid in vacuum obtained by CAM-B3LYP using a variety of Hamiltonians. a) Shows a comparions between 4c and X2C, b) shows a comparison between X2C and SR.

We find that X2C and 4c spectra are more or less identical, while the X2C and scalar-relativistic spectra are significantly different. We then move on to estimate the solvent effects. For this, we carry out molecular dynamics where the test systems are solvated in water. From the trajectories, we extract 500 snapshots. Spectra are calculated for each snapshot, using X2C and CAM-B3LYP, while the water molecules in the environment are modelled by PE. Additionally, EEF effects are included. We then investigate how the average spectrum varies depending on the number of snapshots included, and compare the average of the two isomers of 2-Bromo-2-iodoacetic acid. From this, we find that the average spectra are not properly converged, since the average spectra for the two isomers differ somewhat. However, they are qualitatively similar. Finally, we divide the solvent effects into two parts: a structural perturbation and an electronic effect. The structural effect arises from how the test systems interact with the water molecules in the dynamics simulation. The electronic effect is how the solvent molecules polarize the wave function in the systems and is modelled by PE. We find that both effects are important and that the average spectra including both the electronic and structural perturbation effects yield a surprisingly large difference compared to the average spectrum that only contains the structural perturbation effect.

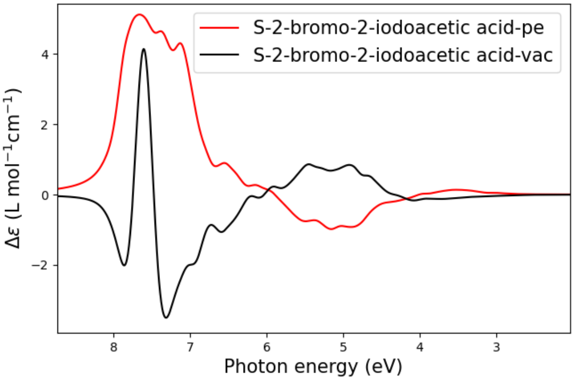

Figure 5.9: Spectra without including PE (black line) and with PE (red line) for the same structures.

5.2 Outlook

In conclusion, the methods in this thesis have been developed to include both a description of solvent effects and a relativistic treatment of the wave function to accurately model spectroscopy. Our studies indicate the success of our methods on the model systems that were employed. We now turn our attention to what could be interesting to explore in future studies. One future direction that would be interesting to pursue, is the development of polarizable density embedding in a relativistic setting. This would alleviate some of the issues that can arise when certain fragments are very close to the QM subsystem (electron spill-out). Another direction would be to extend the polarizable embedding model to work with relativistic coupled cluster. This would enable us to target strongly correlated systems. Moreover, force fields employed for metal complexes are typically not very good, and thus alternative methods to sample structures ought to be explored. Such a method would be to carry out ab initio molecular dynamics.

References

[1] B. Rosenberg, L. Vancamp, J. Trosko, and V. Mansour. 1969.

[2] M. Imran, W. Ayub, I. S Butler, and Z. Rehman. Photoactivated platinum-based anticancer drugs. *Coord. Chem. Rev.*, 376:405–429, 2018.

[3] R. Oun, Y. E. Moussa, and N. J. Wheate. The side effects of platinum-based chemotherapy drugs: a review for chemists. *Dalton Trans.*, 47:6645–6653, 2018.

[4] T. C. Johnstone, K. Suntharalingam, and S. J. Lippard. The next generation of platinum Drugs: targeted Pt(II) agents, nanoparticle delivery, and Pt(IV) prodrugs. *Chem. Rev.*, 116:3436–3486, 2016.

[5] C. Imberti, P. Zhang, H. Huang, and P. J. Sadler. New designs for phototherapeutic transition metal complexes. *Angew. Chem. Int. Ed.*, 59:61–73, 2020.

[6] J. Creutzberg and E. D. Hedegård. Investigating the influence of relativistic effects on absorption spectra for platinum complexes with light-activated activity against cancer cells. *Phys. Chem. Chem. Phys.*, 22:27013–27023, 2020.

[7] L. Ronconi and P. J. Sadler. Unprecedented carbon–carbon bond formation induced by photoactivation of a platinum(iv)-diazido complex. *ChemComm*, 2: 235–237, 2008.

[8] P. J. Bednarski, R. Grünert, M. Zielzki, A. Wellner, F. S. Mackay, and P. J Sadler. Light-activated destruction of cancer cell nuclei by platinum diazide complexes. *Chem. Biol.*, 13:61–67, 2006.

[9] L. Ronconi and P. J. Sadler. Photoreaction pathways for the anticancer complex *trans,trans,trans*-$[\mathrm{Pt(N_3)_2(OH)_2(NH_3)_2}]$. *Dalton Trans.*, 40:262–268, 2011.

[10] A. Y. Sokolov and H. F. Schaefer III. Ground and excited state properties of photoactive platinum (IV) diazido complexes: Theoretical considerations. *Dalton Trans.*, 40:7571–7582, 2011.

[11] H. I. Phillips, L. Ronconi, and P. J. Sadler. Photoinduced Reactions of *cis,trans,cis*-[$Pt^{IV}(N_3)_2(OH)_2(NH_3)_2$] with 1-Methylimidazole. *Chem. Eur. J.*, 15:1588–1596, 2009.

[12] L. Salassa, H. I. A. Phillips, and P. J Sadler. Decomposition pathways for the photoactivated anticancer complex *cis,trans,cis*-[$Pt(N_3)_2(OH)_2(NH_3)_2$]: insights from dft calculations. *Phys. Chem. Chem. Phys.*, 11:10311–10316, 2009.

[13] L. Freitag and L. González. The role of triplet states in the photodissociation of a platinum azide complex by a density matrix renormalization group method. *J. Phys. Chem. Lett.*, 12:4876–4881, 2021.

[14] T. Helgaker, P. Jørgensen, and J. Olsen. *Molecular Electronic-Structure Theory*. Wiley, 2004.

[15] T. Saue. Relativistic hamiltonians for chemistry: A primer. *ChemPhysChem*, 12 (17):3077–3094, 2011.

[16] F. Jensen. *Introduction to Computational Chemistry*. John Wiley Sons, Inc., Hoboken, NJ, USA, 2006. ISBN 0470011874.

[17] T. Saue and T. Helgaker. Four-component relativistic kohn–sham theory. *J. Comput. Chem*, 23:814–23, 2002.

[18] M. Gell-Mann. The interpretation of the new particles as displaced charge multiplets. *Nuovo Cim.*, 4(S2):848–866, 1956.

[19] A. K. Rajagopal and J. Callaway. Inhomogeneous electron gas. *Phys. Rev. B*, 7: 1912–1919, 1973.

[20] A. Dreuw and M. Head-Gordon. Failure of time-dependent density functional theory for long-range charge-transfer excited states: the zincbacteriochlorin–bacteriochlorin and bacteriochlorophyll–spheroidene complexes. *J. Am. Chem. Soc*, 126(12):4007–4016, 2004.

[21] A. Warshel and M. Levitt. Theoretical studies of enzymic reactions: Dielectric, electrostatic and steric stabilization of the carbonium ion in the reaction of lysozyme. *J. Mol. Biol*, 103(2):227 – 249, 1976.

[22] H. M. Senn and W. Thiel. Qm/mm methods for biomolecular systems. *Angew. Chem. Int.*, 48(7):1198–1229, 2009.

[23] S. Ahmadi, L. Barrios Herrera, M. Chehelamirani, Jiří Hostaš, S. Jalife, and D. R. Salahub. Multiscale modeling of enzymes: Qm-cluster, qm/mm, and qm/mm/md: A tutorial review. *Int. J. Quantum Chem.*, 118(9):e25558, 2018.

[24] D. Loco, É. Polack, S. Caprasecca, L. Lagardère, F. Lipparini, JP Piquemal, and B. Mennucci. A qm/mm approach using the amoeba polarizable embedding: From ground state energies to electronic excitations. *J. Chem. Theory Comput.*, 12(8):3654–3661, 2016.

[25] D. Loco, L. Lagardère, S. Caprasecca, F. Lipparini, B. Mennucci, and JP Piquemal. Hybrid qm/mm molecular dynamics with amoeba polarizable embedding. *J. Chem. Theory Comput.*, 13(9):4025–4033, 2017.

[26] Ja. Dziedzic, Y. Mao, Y. Shao, J. Ponder, T. Head-Gordon, M. Head-Gordon, and C. K Skylaris. Tinktep: A fully self-consistent, mutually polarizable qm/mm approach based on the amoeba force field. *J. Chem. Phys.*, 145(12):124106, 2016.

[27] M. Bondanza, M. Nottoli, L. Cupellini, F. Lipparini, and B. Mennucci. Polarizable embedding qm/mm: the future gold standard for complex (bio)systems? *Phys. Chem. Chem. Phys.*, 22:14433–14448, 2020.

[28] J. M. Olsen, K. Aidas, and J. Kongsted. Excited states in solution through polarizable embedding. *J. Chem. Theory Comput.*, 6(12):3721–3734, 2010.

[29] P. Söderhjelm, C. Husberg, A. Strambi, M. Olivucci, and U. Ryde. Protein influence on electronic spectra modeled by multipoles and polarizabilities. *J. Chem. Theory Comput.*, 5(3):649–658, 2009.

[30] A. J. Stone Stone. *The theory of intermolecular forces*. 1997.

[31] L. Gagliardi, R. Lindh, and G. Karlström. Local properties of quantum chemical systems: The loprop approach. *J. Chem. Phys.*, 121(10):4494–4500, 2004.

[32] J. M. H. Olsen. Development of Quantum Chemical Methods towards Rationalization and Optimal Design of Photoactive Proteins. 2014.

[33] J. Applequist, J. R. Carl, and K. Fung. Atom dipole interaction model for molecular polarizability. application to polyatomic molecules and determination of atom polarizabilities. *J. Am. Chem. Soc.*, 94(9):2952–2960, 1972.

[34] E. D. Hedegård, R. Bast, J. Kongsted, J. M. H. Olsen, and H. J. Aa. Jensen. Relativistic polarizable embedding. 13(6):2870–2880, 2017.

[35] I. Harczuk, O. Vahtras, and H. Ågren. Frequency-dependent force fields for qmmm calculations. *Phys. Chem. Chem. Phys.*, 17:7800–7812, 2015.

[36] M. S. Nørby, O. Vahtras, P. Norman, and J. Kongsted. Assessing frequency-dependent site polarisabilities in linear response polarisable embedding. *Mol. Phys.*, 115:39–47, 2017.

[37] A. Wildman, G. Donati, F. Lipparini, B. Mennucci, and X. Li. Nonequilibrium environment dynamics in a frequency-dependent polarizable embedding model. *J. Chem. Theory Comput.*, 15:43–51, 2019.

[38] J. Olsen and P. Jørgensen. Linear and nonlinear response functions for an exact state and for an mcscf state. *J. Chem. Phys.*, 82(7):3235–3264, 1985.

[39] T. Helgaker, S. Coriani, P. Jørgensen, K. Kristensen, J. Olsen, and K. Ruud. Recent advances in wave function-based methods of molecular-property calculations. *Chem. Rev.*, 112(1):543–631, 2012.

[40] O. Christiansen, P. Jørgensen, and C. Hättig. Response functions from fourier component variational perturbation theory applied to a time-averaged quasienergy. *Int. J. Quantum Chem.*, 68(1):1–52, 1998.

[41] P. Salek, T. Helgaker, and T. Saue. Linear response at the 4-component relativistic density-functional level: Application to the frequency-dependent dipole polarizability of hg, auh and pth2. *J. Chem. Phys.*, 311:187–201, 2005.

[42] T. Saue and H. J. Aa. Jensen. Linear response at the 4-component relativistic level: Application to the frequency-dependent dipole polarizabilities of the coinage metal dimers. *J. Chem. Phys.*, 118(2):522–536, 2003.

[43] K. Kristensen, J. Kauczor, T. Kjærgaard, and P. Jørgensen. Quasienergy formulation of damped response theory. *J. Chem. Phys.*, 131(4):044112, 2009.

[44] P. Norman, D. Bishop, H. J. Aa. Jensen, and J. Oddershede. Near-resonant absorption in the time-dependent self-consistent field and multiconfigurational self-consistent field approximations. *J. Chem. Phys.*, 115:10323–10334, 2001.

[45] J. Kauczor and P. Norman. Efficient calculations of molecular linear response properties for spectral regions. *J. Chem. Theory Comput.*, 10(6):2449–2455, 2014.

[46] V. Sébastien, T. Saue, and P. Norman. Linear complex polarization propagator in a four-component kohn–sham framework. *J. Chem. Phys.*, 133:064105, 08 2010.

[47] P. Norman, D. M. Bishop, H. J. Aa. Jensen, and J. Oddershede. Nonlinear response theory with relaxation: The first-order hyperpolarizability. *J. Chem. Phys.*, 123(19):194103, 2005.

[48] L. Rosenfeld. Quantenmechanische theorie der natürlichen optischen aktivität von flüssigkeiten und gasen. *Zeitschrift für Physik*, 52:649–658, 1929.

[49] Joel Creutzberg and Erik. D. Hedegård. Polarizable embedding complex polarization propagator in four- and two-component frameworks. *Journal of Chemical Theory and Computation*, 18(6):3671–3686, 2022.

Scientific publications

Author contributions

Paper i: Investigating the influence of relativistic effects on absorption spectra for platinum complexes with light-activated activity against cancer cells

I carried out the main part of the calculations, participated in writing the manuscript

Paper ii: Polarizable embedding complex polarization propagator in a four- and two-component frameworks

I participated in developing the theory and implementation, carried out all calculations and participated in writing the manuscript

Paper iii: New relativistic quantum chemical methods for understanding light-induced therapeutics

I participated in writing the manuscript

Paper iv: A method to capture the large relativistic and solvent effects on UV-vis spectra of photo-activated metal complexes

I designed the study, carried out the calculations and wrote the first draft

Paper v: Electronic Circular Dichroism at the level of four-component Kohn–Sham density functional theory

I participated in carrying out the calculations and writing the manuscript

Paper vi: A method to explore the combined impact of relativistic and solvent effects on electronic circular dichroism spectra

I designed the study, developed the theory, carried out the calculations and wrote the first draft